Supplementary Materials for

Chromosome errors in human eggs shape natural fertility over reproductive life span

Jennifer R. Gruhn*, Agata P. Zielinska*, Vallari Shukla*, Robert Blanshard*, Antonio Capalbo, Danilo Cimadomo, Dmitry Nikiforov, Andrew Chi-Ho Chan, Louise J. Newnham, Ivan Vogel, Catello Scarica, Marta Krapchev, Deborah Taylor, Stine Gry Kristensen, Junping Cheng, Erik Ernst, Anne-Mette Bay Bjørn, Lotte Berdiin Colmorn, Martyn Blayney, Kay Elder, Joanna Liss, Geraldine Hartshorne, Marie Louise Grøndahl, Laura Rienzi, Filippo Ubaldi, Rajiv McCoy, Krzysztof Lukaszuk, Claus Yding Andersen, Melina Schuh, Eva R. Hoffmann†

*These authors contributed equally to this work.
†Corresponding author. Email: eva@sund.ku.dk

Published 27 September 2019, *Science* **365**, 1466 (2019)
DOI: 10.1126/science.aav7321

This PDF file includes:

Other Supplementary Materials for this manuscript include the following:
(available at science.sciencemag.org/content/365/6460/1466/suppl/DC1)

Materials and Methods

SUPPLEMENTAL MATERIALS

1. Ethics, informed patient consent, and personal data protections.

1.1 Ethics

All research was conducted under national guidelines and legal regulation in their respective countries after approval by the relevant ethics boards. The study at GENERA was approved by the Institutional Review Board of Clinica Valle Giulia to Prof. Ubali and Dr. Rienzi in accordance with Italian law. The studies in Copenhagen at the LRB and Herlev were approved by the Videnskabsetisk Komite in accordance with Danish National regulation (H-2-2011-044; extension license amm. Nr. 51307; license holder: Claus Yding Andersen and H-1604473; license holder: Eva Hoffmann). The research use of oocytes at University Hospitals Coventry and Warwickshire NHS Trust was approved by Coventry and Warwickshire Research Ethics Committee (Chief Investigator: Geraldine Hartshorne, 04/Q2802/26) on 5 June 2004 and amended to include University of Sussex on 2 November 2012. This approval remains current and is updated at least 3-yearly in line with renewals of the associated Human Fertilisation and Embryology Authority Research Licence (Person Responsible: Geraldine Hartshorne, R0155, 1 October 2004 – 31 October 2020). The research use of human oocytes in Dr Schuh's lab has been approved by the UK's National Research Ethics Service under the REC reference 11/EE/0346 (IRAS Project ID 84952, Chief Investigator: Dr Melina Schuh), the Ethics Committee of Lower Saxony (Ärtzekammer Niedersachsen) under the reference 15/2016.

1.2 Recruitment and informed consent

Recruitment and informed consent procedures followed national standards, including the option to withdraw consent at any time during the study, without this having any bearing on clinical treatment. No women or parents/guardians of girls under the age of 18 years withdrew their informed consent. Processing of personal data, including extensive genome sequences were approved by the National Data Agency (Datatilsynet; approval SUND-60-2016 to Eva Hoffmann).

1.3 Anonymity and blinded processing of oocytes

To ensure anonymity, independent clinicians encoded the oocytes with an ID prior to transfer for processing. Data processing was carried out blinded. No personal data other than age of the donor and reason for treatment were transferred from the clinics to the researchers. Clinical data made available for analysis included FSH and number of oocytes retrieved. The informed consent and ethics licenses contain pathways to address handling and patient choice over notification of incidental findings associated with extensive genome sequencing. Next-generation sequencing was done at a low pass (0.01× of nuclear genome in PB1; 0.006× in MII oocyte genome since 30% of reads are mitochondrinal), which is sufficient to allow alignment to the human genome hg19. No variant callings were made.

1.4 Avoidance of self-identification of patients

The nature of our study, especially at the LRB where some of the participants were very young and had rare disorders, poses a significant risk for self-identification in the study. To avoid this, we binned the ages and do not show any specific ages in the supplemental data. However, the majority of our data analyses were carried out with age as a continuous factor as mentioned throughout the manuscript and the Statistics section below. To minimize further the risk of self-identification, participants did not know whether their oocytes were assigned to this study or other studies permitted under the Ethics license (Hoffmann).

2. Collection and IVM of oocytes from human ovarian tissue (cohort 1).

Human small antral follicles were isolated from a total of 145 unstimulated girls and women aged 2.5 to 38.8 years, of which we matured 2,615 GV oocytes from 118 individuals (cohort 1, **table S2**). The remaining 648 GV oocytes from 27 patients were assigned to a different experimental maturation protocol and not included in our analysis. Each patient was undergoing fertility preservation due to diagnoses requiring chemotherapeutic treatment. We included patients with blood disorders and cancers (excluding ovarian) that do not influence ovarian function (*30*). We then categorized patients into the following groups: blood disorder, breast cancer, non-breast

cancer, or other (**fig. S4**). Similar oocytes from unstimulated women have been used for aneuploidy studies prior to IVF becoming widely available (*31-33*) and, more recently, embryo formation and live births after *in vitro* maturation have been reported (*34-37*)

The small antral follicles were collected in conjunction with ovarian cortex cryopreservation procedures at the local hospital. Ovarian tissue was surgically removed by the collaborating hospital, and transported on crushed ice to the Laboratory of Reproductive Biology, National Hospital, Denmark (LRB). The transport time ranged from 10 min. (local surgery on site) to 2-5 hours (Malmö, Odense, Aarhus). No difference in maturation rates were identified between source locations (**fig. S5**). The LRB staff bisected each ovary or ovarian tissue in dishes of saline solution and removed the inner medulla until the ovarian cortex was at a thickness of 1 mm and was ready to be vitrified for fertility preservation. Subsequently, we examined the medulla fragments suspended in the saline dishes at 3-4× magnification to identify and collect cumulus-oocyte-complexes. The oocytes were collected in 4-well dishes of pre-warmed oocyte holding media consisting of McCoy's 5α media containing 25 mM HEPES (Invitrogen, GIBCO) supplemented with 5 mg/ml human serum albumin (HSA, CSL Behring 20%, Marburg, Germany), 2 mM Glutamax (Invitrogen, GIBCO), 0.05 mg/ml penicilin/streptomycin (Invitrogen, GIBCO), and 1 0mg/ml insulin, 5.5 mg/ml transferrin, 6.7 ng/ml selenium (ITS, Invitrogen, GIBCO). Cumulus-oocyte-complexes were classified as "large", "small", or "naked" based on the density of cumulus cells surrounding the oocytes as shown in **fig. S6** (*38*). The cumulus-oocyte-complexes were then placed into *in vitro* maturation (IVM) media for 48 hours, after which the cumulus cells were removed and the oocytes were assessed for maturation (GV, MI, or MII; Section 4).

For IVM, cumulus-oocyte-complexes were washed in LAG media (Origio A/S,) before being moved to the appropriate IVM treatment media. Cumulus-oocyte-complexes were cultured for 48 hours in 20 µl drops of IVM media overlaid with liquid paraffin (Origio A/S) preequilibrated in 5% CO_2, 20% O_2, at 37 °C for a minimum of 4 hours. The basic IVM media contained IVM media (Origio A/S), 75 mIU/ml rFSH (Puregon; MSD, Oss, the Netherlands), 100 mIU/ml rLH (Luveris, Merck, Copenhagen, Denmark), and 10 mg/ml HAS (Irvine Scientific) (*38*). Some of the cumulus-oocyte-complexes were treated with salubrinal, midkine, and amphiregulin as a part of an independent study to improve maturation rates. These treatments did not affect aneuploidy rates in the oocytes that we tested.

3. Collection and oocytes from gonadotrophin-stimulated women (cohort 2).

At all IVF/fertility clinics, patient treatment occurred independently of participation in our study. We collected GV, MI and MII oocytes at INVICTA, Poland. At GENERA, Italy, and Warwick, UK we collected only GV and MI oocytes. A total of 1,201 MII, 186 MI, and 272 GV oocytes were collected from 123 patients across the three clinics (**table S3**). Of these samples, 322 oocytes from 85 patients (19-42 years) were donated to the project. This included 84 *in vivo* matured metaphase II-arrested (MII) oocytes from INVICTA that are normally used in fertility treatment, but were donated for research. The remaining 238 oocytes were GVs that were matured *in vitro* after removal of the cumulus/granulosa cells. This population is similar to *in vivo* matured MII oocytes in terms of aneuploidy (*8, 9*). An initial pilot study found that oocytes in MI at the time of collection had elevated levels of aneuploidy and were therefore not used in this study. In addition, we also used data from a previously published study of *in vivo* matured MII oocytes (**table S4**) (*14, 15*).

3.1 GENERA- GEN

At GENERA, Italy, the patients who donated immature oocytes to this study underwent controlled ovarian stimulation according to (*39*). Transvaginal ultrasound and serum oestradiol concentrations were used to monitor the cycle. Final follicular maturation was induced with the administration of 10,000 IU of hCG (Gonasi; IBSA, Switzerland) or a single subcutaneous bolus of GnRH agonist (50 IU Buserelin; Sanofi-Aventis, Canada) when at least three follicles reached an average diameter >17 mm. The cumulus–oocyte complexes were aspirated 36hr after the ovulation trigger. After 2hr of incubation in a controlled atmosphere (6% CO_2 and 5% O_2), the oocytes were denuded in HEPES-buffered medium (Irvine Scientific, USA) supplemented with 5% Human Serum Albumin (HSA, Irvine Scientific) and containing 20 IU/ml of hyaluronidase (Hyaluronidase Solution 80 IU/ml, Irvine Scientific). After the decumulation, the maturation status of the oocytes was evaluated. For MII oocytes, ICSI was performed immediately, while the immature oocytes (GV and MI) were vitrified. When needed, vitrified GV and MI oocytes were thawed and cultured at 37 °C in a controlled atmosphere (6% CO_2 and 5% O_2) in a continuous

single step medium (CSCM, Irvine Scientific) overnight. After 24hr, the oocytes that managed to mature to the MII stage were isolated for NGS analysis or spread.

The vitrification and warming procedures were performed using commercially available kits (vitrification and warming kit, Kitazato BioPharma Co, Japan), with a few modifications described in Rienzi *et al.* (2010) (*40*). Briefly, the vitrification procedure was performed at room temperature. The oocytes were initially moved from the culture medium to the HEPES-buffered medium (Irvine Scientific, USA) supplemented with 5% Human Serum Albumin (HSA, Irvine Scientific), then to perform the equilibration gradually, this was balanced with a solution of equilibration solution (ES) containing 7.5% ethylene glycol (EG) and 7.5% dimethylsulfoxide (DMSO) in HEPES-buffered basic culture medium M-199 with 20% synthetic serum substitute (SSS) for 12 min. The oocytes were then transferred in 1ml of vitrification solution containing 15% EG, 15% DMSO and 0.5M sucrose in M-199 with 20% SSS for 1 min. The oocytes were then placed on the Cryotop strip (Kitazato) surrounded by a minimal volume of VS. The devices were lastly plunged into liquid nitrogen. For the warming procedure, the first step is performed at 37 °C. The cap was removed in liquid nitrogen and the Cryotop was immediately submerged in 1 ml of warming solution (WS) containing 1.0 M sucrose in M-199 with 20% SSS. After 1 min, the oocytes were placed in 1 ml solution containing 0.5 M sucrose, and incubated at room temperature for 3 min. Finally, the oocytes were washed at room temperature for 3 min. in 1 ml basic medium M-199 + 20% SSS , and then transferred into 1 ml in a culture medium (CSCM, Irvine Scientific). Degenerated oocytes were removed from the cohort that was submitted to PB1 biopsy, oocyte activation and PB2 biopsy.

3.2 INVICTA- VIC

At INVICTA, Poland (VIC), oocytes were collected by surgical means approximately 35 hours post LH surge or administration of human chorionic gonadotrophin (hCG) injection. On the day of oocyte retrieval, following removal of cumulus cells and cells of the corona radiata, all oocytes identified as immature (GV or MI) were placed in pre-warmed pre-equilibrated (minimum 3 hours) G-1 culture media (Vitrolife) under oil and incubated at 37 °C with 6% CO_2 and 5% O_2 for 24 hours. Following overnight culture, the maturation status of each egg was observed and recorded. Oocytes were then vitrified using commercially available kits and protocol (vitrification kit,

Kitazato BioPharma Co, Japan). The corresponding Kitizato warming kit was used on day of processing and the oocytes moved again to G-1 media after thawing. Oocytes that underwent biopsy were moved to dishes of G-PGD media (Vitrolife).

3.3 Warwick-WAR

Patients at Warwick, UK (WAR) received ovarian stimulation and underwent IVF treatment using standard protocols. On the day of oocyte retrieval and following cumulus removal, all oocytes identified as immature (GV or MI) prior to ICSI injection were incubated under oil in 100uL drops of culture media (ORIGIO Sequential Cleav media) in a 5% O_2, 6% CO_2, 89% N_2 gas mixture at 37 ^oC. Following overnight culture, the maturation status of each egg was observed and recorded.

4. Determining maturation and activation rates.

4.1 Maturation rates (meiosis I).

Maturation rates to metaphase stage of meiosis II (MII) were determined by assessing the disappearance of a GV nucleus followed by extrusion of the first polar body (PB1). We scored oocytes that had resumed meiosis I as MI (no GV, no PB1). The MI population is a mixture of oocytes with GVBD that may have arrested before spindle formation; are in MI or arrested in MI; as well as MII oocytes, but with failed PB extrusion. The data on GVBD for cohort 1 are shown in Fig. S2. For cohort 2, GV oocytes obtained from stimulated women in IVF clinics, GVBD rates were as follows: 18 out of 26 (69%; GENERA), 92 of 180 (51%; INVICTA) and 17 of 32 (53%, Warwick), or overall 53% (n= 238) (**fig. S7A**).

4.2 Artificial activation rates (meiosis II).

To assess completion of meiosis II, which is normally triggered by fertilization, we used an artificial activation method that we previously developed and verified does not interfere with chromosome segregation at meiosis II (PB2 extrusion) (*15*, *41*, *42*). Thus, no oocytes were fertilized by sperm in our studies. Briefly, we exposed *ex vivo* matured or *in vivo* matured oocytes to 100 µM A23187 (Sigma, A23187) for 40 min. and assessing female pronucleus and PB2

extrusion after 24 hours. After activation, oocytes were incubated in Quinn's Advantage cleavage medium (Sage, USA) supplemented with 10% HSA at 5% O_2, 5% CO_2, 37 °C under oil.

5. Development of MDA-NGS pipeline for chromosome copy number analysis.

5.1 Whole genome amplification by multiple displacement amplification (MDA).

Sample amplification by multiple displacement amplification (MDA), was performed using the SureMDA DNA Amplification System (Illumina Inc.), according to the Infinium™ Karyomapping Assay Protocol Guide (15052710 Rev.B; Illumina Inc.). Reactions were performed in thin-walled 0.2 ml PCR tubes. Human euploid male genomic DNA (G1471, Promega) was quantified using the Quant-iT dsDNA High-Sensitivity (HS) Assay Kit (ThermoFisher Scientific), and 50 pg in a final volume of 4 µl 1× PBS was used for positive amplification control. 4 µl 1×PBS was used as a negative 'no template' control (NTC). All sample pipetting steps were performed over a pre-cooled, -20 °C tube rack (Eppendorf) in a Class II Microbiological Safety Cabinet within a designated pre-PCR laboratory. Reagents were dispensed onto the inner wall of each sample tube above the droplet containing the sample, so as not to remove the sample material when withdrawing the pipette tip. Reagents were collected at the bottom of each tube by centrifugation at 280 ×*g* for 5 sec. Immediately before use, single cell samples were removed from -20 °C storage and centrifuged at 300 ×*g* for 3 min. MDA lysis and amplification reactions were assembled according to the manufacturer's instructions. Heating steps were performed using a Veriti™ 96-Well Fast Thermal Cycler (ThermoFisher Scientific). During addition of neutralisation buffer post-lysis, the sample tube rack was periodically tapped on the work surface to collect reagents together. Samples were amplified for 2 hours at 30 °C in a post-PCR laboratory. SureMDA products were stored at -20 °C prior to resolution by gel electrophoresis and quantitation of duplex DNA.

5.2 Quality assessment of whole-genome amplified DNA samples.

Amplified DNA quality was assessed by DNA quantitation and fragment analysis. MDA products including cell collection and amplification controls, were resolved by gel electrophoresis to assess signs of amplification, and further quantified using the Quant-iT dsDNA High-Sensitivity (HS)

Assay Kit (ThermoFisher Scientific) according to the manufacturer's instructions, following dilution 1:80 in Resuspension Buffer (Illumina Inc.). Following PCR amplification during NGS library preparation, samples were diluted 1:4 and assessed using the same Quant-iT method. The Quant-iT assay plates were analysed using a FLUOStar® Omega Plate Reader and FLUOStar® Mars Data Analysis software (BMG Labtech, Germany).

Automated electrophoresis was used for high-sensitivity quality control of fragmented DNA during library preparation for NGS. Libraries were analysed following PCR-mediated addition of barcode indices. Samples were diluted in Resuspension Buffer (Illumina Inc.) to fall within the detection limit of the assay, and analysed using the Agilent High Sensitivity DNA Kit (Agilent) on a 2100 Bioanalyzer instrument and 2100 Expert software (Agilent).

6. Copy number variation detection in SureMDA products

Preparation of NGS libraries was performed using commercially available kits and reagents with some workflow modifications. The following describes a custom NGS library preparation workflow for genomic content analyses of single cells by copy number variation detection. Libraries were sequenced using a MiSeq® System (Illumina Inc.) (Fig 2A). We adapted the workflow to give a 0.01× coverage in single cells. However, for the MII oocytes, mitochondrial reads (30%) render the total coverage lower (0.006×), without affecting precision.

6.1 Sample input

MDA products from single cells were quantified according to Quant-iT method described previously and diluted to a final concentration of 5 ng/µl in Resuspension Buffer (RSB) (Illumina Inc.).

6.2 Tagmentation

Each library was tagmented according to the Nextera® DNA Library Prep Reference Guide (15027987 v01; Illumina Inc., CA, USA) with the following modification; 100 ng MDA product

in 20 µl RSB was used for sample input. Tagmentation was stopped by addition of 5 µl Stop Tagment (ST) reagent to each sample as described in the manufacturer's protocol.

6.3 Clean-up tagmented DNA

Tagmented DNA was cleaned up by 1.8× Solid Phase Reversible Immobilisation (SPRI) on Sample Purification Beads (SPB), according to the Nextera® Rapid Capture Enrichment Reference Guide (15037438 v01; Illumina Inc.), with the following modifications: Clean-up was performed in a 0.8 ml 96-well midi plate (AB-0859; ThermoFisher); 90 µl SPB and 50 µl of each tagmented DNA library was used as input for clean-up; following removal of 80% ethanol, samples were dried on a heat block (UY-36620-05; Bio-Techne,) set to 50 °C for 5 min; samples were resuspended in 25 µl RSB, and 20 µl cleaned-up supernatant was transferred to a 0.2 ml 96-well PCR plate (AB-600-L; ThermoFisher Scientific) for PCR.

6.4 PCR amplify tagmented DNA

DNA libraries were amplified and barcoded by PCR according to the Nextera® Rapid Capture Enrichment Reference Guide (15037438 v01; Illumina Inc.), with the following modifications: Indexes used were of the 96-sample NextSeq Index Kit (20000440; Illumina Inc.); PCR amplification master mix was NLM (15037037; Illumina Inc.), with the following PCR program: 72 °C for 3 min, 98 °C for 3 min followed by 10 cycles of [98 °C for 30 sec, 60 °C for 30 sec, 72 °C for 3 min] then 72 °C for 5 min and hold at 10 °C.

6.5 Clean-up amplified DNA

PCR products were cleaned-up 1× SPRI on SPB, according to the VeriSeq® PGS Library Prep Reference Guide (15052877 v03; Illumina Inc.) with the following modification: Following removal of 80% ethanol, samples were dried on a heat block (Bio-Techne) set to 50 °C for 5 min. Cleaned-up amplified libraries were quantified using the Quant-iT method described previously. Samples with a concentration ≥5 ng/µl were used for normalisation.

6.6 Normalise and pool libraries

Cleaned-up amplified DNA was subjected to bead-based normalisation as described in the VeriSeq® PGS Library Prep Reference Guide (15052877 v03; Illumina Inc.) without modification. Libraries were pooled by addition of 5 µl each normalised library to a 1.5 ml LoBind microcentrifuge tube (Eppendorf). The library pool was mixed by pulse vortexing and centrifugation, before aliquoting into single-use 0.2 ml PCR tubes in 20 µl volumes. Library pool aliquots were kept on wet ice or stored at -20 °C until sequencing.

6.7 Sequencing on MiSeq System

Pooled libraries were sequenced using a MiSeq® instrument (SY-410-1003; Illumina Inc.) with MiSeq Reagent Kit V3 consumables (Illumina Inc.). 8-15 µl of library pool was denatured in a final volume of 100 µl Hybridisation Buffer (Illumina Inc.) at 96 °C for 3 min and cooled to 4 °C on a Veriti™ Thermal Cycler (ThermoFisher Scientific). The input volume of library pool was adjusted for a target cluster density of 1200-1400 K clusters/mm^2. 100 µl denatured library pool was added to 600 µl Hybridisation Buffer, that had been pre-cooled on wet ice in a 1.5 ml DNA LoBind microcentrifuge tube (Eppendorf); vortexed and pulse centrifuged. 600 µl of denatured, diluted library pool was analysed by paired-end sequencing of 36 bases (2×36 bp) using V3 Amplicon chemistry.

6.8 Primary analysis and generation of an MDA-specific database for NGS

Primary analysis of NGS data is performed onboard the MiSeq instrument using the MiSeq Reporter software. Cluster density, total reads, reads passing filter and Q30 quality scores were assessed for library QC. Binary sequence alignment map files (*.bam) were used for secondary analysis. A reference database for CNV analysis was created using NGS data (*.bam files) derived from 96 SureMDA-amplified euploid male gDNA (Promega) samples, processed using the same workflow described here, with bioinformatics support from Illumina Inc. The reference database aims to capture systematic assay noise such as GC-bias in DNA amplification, and is compatible BlueFuse® Multi software for CNV analysis (Illumina Inc.).

6.9 Secondary analysis

Secondary analysis was performed using BlueFuse® Multi software (v4.3; Illumina Inc.), using the reference database described here, and designed specifically for use with sequencing data generated from single cells following MDA. Briefly, unmapped reads, duplicate reads, poorly mapped reads were removed, and sequence read counts per bin were normalised for GC content. Bias was removed according to the MDA-specific reference database. Data was smoothed using a multi-bin sliding median and copy number variation was determined using a gaussian probability function (copy numbers 0-4) with a standard deviation of 0.33, assuming the median autosomal read count correlated to a copy number of two. In our case, both normalised and raw aligned sequence counts per bin were used for assessment of copy number variations in each sample.

7. Validation of MDA-NGS sequencing pipeline.

7.1 Source of single cells and gDNA of known karyotype

The MDA-NGS pipeline for CNV detection in single cells was performed using cell lines obtained from the NIGMS Human Genetic Cell Repository at the Coriell Institute for Medical Research, New Jersey, USA. We used cell lines GM00526 (fibroblast, 47, XY, +13) and GM04927 (EBV-transformed lymphoblastoid cell line, 47, XY, +21). The cell lines were cultured in standard medium and single cells were manually isolated as previously described (*43*); cells isolates were stored at 4 °C until WGA, performed on the same day.

7.2 Whole-genome amplification, library preparation and sequencing results

Twelve gDNA replicates and 12 single cells were amplified suing SureMDA and sequenced using the MDA-NGS pipeline described previously. We observed the expected karyotype in 24 out of 24 gDNA samples, and no false positive abnormalities were observed. For single cell isolates (n=12 per cell line), we observed two false positives for each cell line. For GM04927, the two false positives are consistent with the segmental abnormalities, suggesting a false positive rate of 8% (2 of 24). We also observed one false negative, consistent with that chromosome loss occur during cell culture. However, we used a conservative estimate of 4% false negative rate. Due to these rates, we sequenced both the oocyte and PB1, allowing us increased certainly of the aneuploidy

due to the expected reciprocal nature of meiotic errors (i.e., loss in one cell should be accompanied by gain in the other). We estimated the FDR to be less than 3.1×10^{-6} using this approach.

8. SNP array analysis.

Genotype information at single nucleotide polymorphisms (SNP) loci were determined by microarray analysis, using whole-genome MDA products from single cells or bulk genomic DNA extracted from cell lines.

8.1 Infinium™ HumanKaryomap-12 BeadChip Array

Single cell MDA products and gDNA extracted from cell lines were genotyped using the Infinium™ HumanKaryomap-12 DNA Analysis Kit (Illumina Inc.), according to the manufacturer's instructions (15052710 Rev.B; Illumina Inc.). Laboratory equipment required for processing Infinium™ BeadChip arrays is supplied as a single package (WG-15-305; Illumina Inc.).

Briefly, gDNA samples were adjusted to 50 ng/µl in Resuspension Buffer (Illumina Inc.). Single cell MDA products were not diluted. 8 µl of each sample was denatured with ≈0.1 N NaOH (72079; ThermoFisher Scientific) for 10 min prior to isothermal amplification at 37 °C for 2 hours on a Hybex® System (SciGene). Infinium™ amplification products were enzymatically fragmented 37 °C for 30 min and subjected to isopropanol precipitation (I9516; Sigma-Aldrich) by centrifugation at 3000 ×*g* for 20 min at room temperature, before resuspension in supplied hybridisation buffer. Fragmented DNA was denatured at 95 °C for 20 min, and 15 µl of each sample was loaded onto HumanKaryomap-12 v1.0 BeadChip Arrays. Microarray slides were placed inside sealed Illumina hybridisation chambers and incubated overnight in an Illumina hybridisation oven equipped with a rocking table at 48 °C for 16-20 hours.

BeadChip arrays were washed using kit-supplied reagents before assembly into Te-Flow flow-through chambers, and inserted into a Tecan Chamber Rack (Tecan, Switzerland). Single base extension of Infinium™ oligonucleotide probes was performed at 44 °C, prior to denaturation with 95% formamide + 1 mM EDTA. Staining of biotin and dinitrophenyl (DNP) labelled nucleotides

for signal amplification with two-colour master mix and anti-stain was performed at 32 °C. BeadChip arrays were immediately washed and coated before vacuum drying at >0.9 bar for 50 min. Arrays were stored in the dark until scanning.

Processed arrays were scanned using either the iScan® System (Illumina Inc.) or NextSeq® 550 System (Illumina Inc.). The back of each chip was wiped with 70% ethanol to remove residual slide coating and ensure the chips lay flat in the adapter for scanning. Chip-specific DMAP files (*.dmap) were downloaded using DMAP Decode File Client (DFC) Utility Software (v 3.0.2; Illumina Inc.). The intensity data files (*.idat) generated by both scanning systems were converted using AutoConvert software (v2.0.1; Illumina Inc.) or Beeline software (v2.0.3; Illumina Inc.) to generate genotype call files (*.gtc) for analysis. Generation of *.gtc files requires product-specific manifest files (*.bpm) and cluster files (*.egt) for data annotation, available at www.illumina.com.

8.2 Primary analysis of SNP microarray data

Intensity data (*.gtc and *.idat) files were imported into the genotyping module of the GenomeStudio software (v2.0.2; Illumina Inc.) for genotype calling using the Illumina GenCall algorithm. The default GenCall threshold for genotype calling was set at 0.15, and reduced to 0.01 for secondary analysis using SureTypeSC. Total call rates and heterozygous call rates were used to screen sample quality. The full data table was exported in *.csv format for secondary analysis.

8.3 Secondary analysis of SNP microarray data

We used R and SureTypeSC (*44*) in order to conduct secondary analysis of chromosome segregation patterns, especially reverse segregation as described in (*15, 41*).

9. Quality control of MDA-NGS and MDA-SNP analyses from oocyte and polar bodies.

All MDA products from single cell samples from oocyte-PB1 duos were quantified and hybridised to SNP microarrays to assess human genome coverage. In total, 38 out of 307 (12.38% ± 0.94% S.E.P) single cell samples were excluded following SNP array analysis. 35 samples were excluded due to absence of genotype calls in the green channel (C/G bases; B-type). These samples had a

total call rate >60%, but an imbalance in the proportion of AA and BB calls such that <5000 out of 293,869 features were called BB genotype by GenomeStudio software (GenCall threshold: 0.15). This is consistent with the negative control (sample-dependent failure), in which no sample was hybridised to the array prior to washing, staining and scanning. Of these 35 samples, 33 had an MDA yield of <15 µg per 50 µl reaction, with an average of 5.40 µg ± 5.37 S.D. The remaining two samples gave higher MDA yields of >20 µg, however also showed the same failure mode (low B-allele call rate). These two samples were prepared for NGS but subsequently failed to give interpretable CNV results; due to either inaccurate quantification of the MDA product, or non-human contamination during WGA. An additional three samples were excluded following SNP array QC due to suspected human DNA contamination, with call rates that were more consistent with gDNA (total call rate >87% and AB call rate >21%). All remaining samples passed Infinium™ sample-independent controls, indicating no failures during array processing. Sample-dependent Infinium™ controls (GenomeStudio) were not used for QC of MDA products since values are likely to be affected by aneuploidy in the samples. An additional 16 out of 307 samples, which had passed SNP array QC, were excluded from NGS library preparation due to low MDA yield <3 µg, with an average of 1.53 µg ± 0.60 S.D. Thirty-seven out of 253 (14.62% ± 1.11% S.E.P) sequenced samples were excluded due to high noise/uninterpretable CNV traces generated using BlueFuse® Multi software, with the custom MDA reference database described above.

To sum up, 91 out of 307 (29.64% ± 1.30% S.E.P) single cell samples failed to give interpretable CNV traces following DNA content analysis. MDA yield is not representative of genome coverage, and therefore cannot solely indicate sample quality. However, differences in the average MDA yield (µg ± S.D) were observed between oocytes and polar bodies from stimulated cycles (GENERA, 24.18 ± 8.22) and IVM of GV oocytes from small antral follicles (LRB, 13.93 ± 7.59). The difference in pipeline efficiency between clinics was also mirrored in samples failing NGS due to CNV trace noise profiles, in which DLR values were typically higher in oocytes from small antral follicles (cohort 1) than those from stimulated cycles (cohort 2).

In total, 216 samples passed QC criteria for CNV analysis, with comparable sequencing metrics between oocyte/PB samples and single cells isolated from cell lines, respectively; % mapped reads (± S.D) 98.85 ± 0.47 vs. 98.96 ± 0.30 (t-test, p>0.05 n.s); % reads passing filter (± S.D) 80.53 ±

11.68 vs. 89.94 ± 0.84 (t-test, $p<0.001$). The high variability in reads passing filter (%) for oocyte/PB samples may be improved by lowering the cluster density during sequencing. A higher cluster density is likely to be caused by a shorter average fragment size within the library pool, when loading the same volume of library onto the reagent cartridge following bead-based normalisation. Whilst further work would be required to optimise this value, the present number of reads available after filtering is sufficient to perform simple content analysis due to the paired-end sequencing strategy. The DLR values for included samples were typically higher in oocytes following IVM from GV oocytes compared to *in vivo* maturation after ovarian stimulation, as seen for excluded samples. However, for samples passing NGS QC, the average (± S.D) DLR value for cell line isolates was 0.52 ± 0.10 compared to 0.35 ± 0.14 for oocyte and polar body samples from stimulated cycles (t-test, $p<0.001$). Taken together, oocytes and polar body samples show lower MDA bias, and therefore more linear genome coverage compared to single cells isolated from cell line cultures. This is consistent with the notion that oocytes and polar bodies are not in S-phase at the time of biopsy, compared to unsynchronised cells in culture, and therefore we expect to see a higher variation in genome representation in the traces from unsynchronized cells.

Prior to CNV analysis, a further 56 out of 307 (18.24% ± 1.10 S.E.P) samples did not have a matched meiotic cell passing QC to allow reciprocal CNV detection and were also excluded from CNV classification. Taken together the pipeline efficiency for oocytes from stimulated cycles per sample was 83.16% (79 out of 95 single cells), and the matched-cell inclusion efficiency was 80.49% (33 out of 41 oocytes). For oocytes obtained from small antral follicles (cohort 1), the pipeline efficiency per sample was 64.62% (137 out of 212 single cells), and the matched-cell inclusion efficiency was 40.19% (43 out of 107 oocytes).

10. Chromosome spreads from human oocytes.

Single cell metaphase spreads allowed for cytological analysis of both small antral follicles and large antral follicles (**fig. S8**) (*45*). Spreads were made from both MII oocytes either directly after maturation or after thawing of vitrified MII oocytes. A total of 186 oocytes were spread: 128 small antral follicles and 58 large antral follicles (36 matured GVs and 22 MIIs*). We obtained high quality data from 55. The relatively low efficiency is due to oocyte loss during preparation, which

relies on differential swelling and bursting. Some spreads were not appropriate for analysis after staining and were excluded from the final analyses (e.g., **fig. 1B**, **C** and, in particular, **fig. 3A** for measurements of intersister kinetochore distances). To pass quality control the chromosomes needed to adhere to the slide and spread enough that we were able to identify a majority of chromosomes. Chromatid count was completed using centromere number identified by CREST serum signals, including in regions where small clusters of chromosomes failed to separate from one another.

Prior to spreading, 1.5 ml tubes of Tyrode's (Sigma) and 0.9% sodium citrate were pre-warmed to 37 ºC. The following protocol was performed entirely on a 37 ºC heated benchtop. Oocytes were first removed from their holding media (varied by clinic) and placed into a 30µl droplet of pre-warmed Tyrode's to remove the zona. Using a 130-133 µm denudation pipet (Vitrolife), the oocyte was pipetted up and down until the zona tore open and visually disintegrated. Once the zona was removed the oocyte was run through a series of three 30 µl drops of sodium citrate to remove the remaining Tyrode's. The oocyte was then left in the final drop of sodium citrate until it visibly increased in size. Meanwhile, ethanol cleaned microscope slides (Superfrost Plus, ThermoFisher) were prepared with a small circle is etched onto the underside using a diamond pen. The slides were dipped into a formaldehyde solution consisting of 1% formaldehyde (freshly prepared from paraformaldehyde, Sigma), 0.15% Triton-X (Sigma), 3 mM DTT (Sigma), and the pH adjusted to 9.2 using boric acid. Next, the oocyte was dropped onto the slide in the center of the circle with minimal media. Using a stereomicroscope, the spread was determined successful if the oocyte visually burst once making contact with the slide and the cytoplasm dissipated. Slides were then laid flat in a pre-warmed (37 °C) humid chamber and allowed to incubate for a minimum of two hours and a maximum of overnight. After incubation, the humid chamber was opened slightly to allow for slow drying. Once slides were dry they were washed in a 1% Photoflo (Kodak) solution for two minutes to remove residual debris and airdried. Slides were stored at -20 ºC until further processing.

Immunostaining for DAPI and CREST serum (centromeres) was used for aneuploidy and iKT distance analysis. CREST (Antibodies Incorporated, 15-234) was diluted 1:500 in sterile filtered 1× ADB consisting of 2.5 ml normal donkey serum (Sigma), 0.75 g IgG free BSA (Jackson

Immunoresearch), 12.5 µl Triton-X 100 (Sigma), and 22.5 ml PBS. Slides were first blocked in 1× ADB for a minimum of 1 hour before 50 µl antibody was added to the centre of the slide and a parafilm coverslip added. Slides were then placed in a humid chamber with boiling water and incubated for two hours, before moving the humid chamber to 4 °C overnight. Slides were then washed in 1 × ADB for 30 minutes. Alexa Fluor 594-conjugated AffiniPure Donkey Anti-Human IgG (Jackson ImmunoResearch; 1:75) was then added and the slides incubated in a humid chamber with boiling water for two hours in the dark. Incubation was then followed by two consecutive 1 × PBS washes of 30 and 60 minutes. Slides were fixed with ProlongGold antifade with DAPI (Invitrogen), sealed with clear nail polish, and stored at 4 °C until analysis.

11. High resolution imaging of intact human oocytes.

To analyze chromosome morphology during meiosis II, oocytes obtained from women aged between 19 and 46 were fixed using a method that preserves an intact spindle architecture. Oocytes were cultured at 37 °C until the meiosis II stage as previously described (*46*). In brief, following retrieval, oocytes were transported to the research lab and cultured in G-MOPS medium (Vitrolife, #10129) supplemented with 10% FBS (Gibco, #16000044) under mineral oil (Merck, #8012-95-1). Only oocytes that appeared morphologically healthy and underwent NEBD within 24 hours from retrieval were used in the study. To analyze chromosome and kinetochore morphology in meiosis II, the oocytes were fixed at least 4 hours following polar body extrusion. In Fig. S13, oocytes were preserved late in meiosis I as described previously (*20*, *46*). None of the oocytes used for this study were subjected to long-term live imaging before fixation.

Oocytes were fixed for 60 min. at 37 °C in 100 mM HEPES (pH 7), 50 mM EGTA (pH 7), 10 mM $MgSO_4$, 2% formaldehyde (MeOH free) and 0.2% Triton X-100, based on previously published methods (*20, 46*). Some oocytes were additionally subjected to a 6 min. cold-treatment that depolymerizes kinetochore-bound microtubules. After fixation, oocytes were extracted in PBS, 0.1% Triton X-100 overnight at 4 °C. All antibody incubations were performed in PBS, 3% BSA and 0.1% Triton X-100, either overnight at 4 °C (for primary antibodies) or for 3 hr at room temperature (for secondary antibodies). The primary antibodies used were rat anti-α-tubulin (MCA78G, Serotec; 1:3000) and human ACA centromere CREST autoantibody (FZ90C-CS1058,

Europa Bioproducts; 1:1000). As secondary antibodies, Alexa-Fluor-488 labelled anti- human and Alexa-Fluor-647 labelled anti- rat were used. DNA was stained with 0.5 µg/ml Hoechst 33342 (Molecular Probes).

To establish the fraction of oocytes that exhibited discernible chromatin threads between the two meiosis II chromatids (**fig. 4**) MII oocytes were imaged using AiryScan super-resolution microscopy. Images were acquired using the AiryScan module on Zeiss LSM800 and LSM880 microscopes equipped with 40× C-Apochromat 1.2 NA water-immersion objectives and processed post-acquisition using ZEN2. Spatial resolution was 0.19 µm optical sections, covering the entire spindle. To ensure a reliable assessment of chromosome morphology, each oocyte was manually rotated prior to image acquisition using a tip of a blunt glass capillary, so that the long axis of the spindle was in parallel to the plane of the imaging dish (*46*).

In order to assess quantitatively the separation of sister kinetochores and score for the presence of gaps in Hoechst signal between chromatids in meiosis II (**fig. 4A-C**), kinetochore separation at MII was determined by a 3D analysis in Imaris, Bitplane. First, the two kinetochores belonging to the same chromosome were identified by comparing CREST and Hoechst staining in consecutive z-planes spanning the entire chromosome. The center of each kinetochore was then detected using an automated spot detection function based on local maxima in Imaris (Bitplane). The distances between the sister kinetochores were measured in Microsoft Excel using the xyz coordinates of kinetochore centers defined by the automated spot detection function in Imaris (Bitplane). Sister kinetochores were frequently detected in different z-sections and the Pythagorean Theorem was used to calculate the distances between all kinetochore pairs. Oocytes evaluated for this purpose were imaged as described above or using Zeiss LSM710 confocal microscope equipped with a 63× C Apochromat 1.2 NA water immersion objective at a spatial resolution of 0.3 µm optical sections and deconvolved using Huygens Professional (Scientific Volume Imaging). All distances and kinetochore configurations were determined blindly to donor's age. The quantifications were further confirmed by an independent second count.

12. Statistical methods.

12.1 General statistical methods.

We followed the guidelines from the American Statistical Association regarding biological inference from p-values, effect size and power of detection (*47*). We used R (www.r-project.org) (*48*) and conducted generalized linear models (GLM) with maternal age group as an independent categorical variable for the majority of figures, as described. We have reported effect size, power, and p-values for statistical models (summarized in **table S8**). For GLMs, we used the measured explained variation, analogous to linear regression R^2, referred to as pseudo R2 throughout (*49*).

*12.2 Meiotic errors and aneuploidy in human oocytes (**fig. 1B and C**).*

We obtained chromosome content data from 218 meiosis I, covering 5,014 chromosome segregation events. We used a generalized linear model (GLM) to assess whether technology (chromosome spread, sequencing or SNP arrays), source (cohort 1 or cohort 2), maturation method (*in vitro* or *in vivo*), and maternal age influenced aneuploidy incidence either per oocyte (GLM; family = binomial; **fig. 1B**) or meiosis I errors as a proportion of chromosomes (GLM; family = quasibinomial; **fig. 1C**). Female age was the only explanatory variable with a significant effect on aneuploidy both when oocytes (**fig. 1B**) or chromosomes (**fig. 1C**) were considered (**table S8**). We therefore pooled the oocytes from cohort 1 and cohort 2 to obtain maximal power of detection and used maternal age as a continuous, explanatory variable in subsequent GLMs. Where possible, we ascertained that both cohorts showed similar effects. We compared linear, quadratic and third order polynomial GLMs using ANOVA and χ^2 statistics as well as the AIC. The rsq package in R was used to calculate explained variation of the model. Since data were relatively sparse, we used a graphical representation of the incidence of aneuploidy and meiotic errors, using bar graphs (**fig. 1B**, **C**) that were overlaid on the graph of the fitted values of the best-fit model.

12.3 Predicted aneuploidy rates in conceptions based on human oocyte data.

To understand how meiosis I errors would result in aneuploid conceptions, we modelled the anticipated error rates after the second division, which normally occurs upon fertilization. Notwithstanding a small incidence of meiosis II errors that would affect meiosis I nondisjunction and PSSC equally, aneuploidy rates in human conceptions would be dependent upon the risk associated with a meiosis I nondisjunction (100%); PSSC (50%): and reverse segregation (25%).

We used binomial to calculate the overall risk of having an aneuploid conception (0 to 1), depending upon whether one or more chromosomes had mis-segregated during meiosis I.

*12.4 Analysis of genetic data from preimplantation embryos (**fig. 1E**)*

Within the PGT-A data (**fig. 1E** and **fig. S12**), putative meiotic-origin chromosome gains were distinguished based on inferred patterns of maternal chromosome transmission. Specifically, detection of both maternal haplotypes—a signature we term 'both parental homologs' or 'BPH'—in any chromosomal region of the embryonic genome serves as an indicator of meiotic-origin trisomy or, rarely, uniparental disomy (*10, 11*). We note that this signature does not capture meiotic-origin chromosome losses, nor does it capture meiosis II chromosome gains in the absence of recombination (*10, 11*).

For each PGT-A case, we counted embryonic samples exhibiting one or more maternal BPH chromosome gain, as well as embryonic samples lacking this signature across all chromosomes. We then used a quasibinomial generalized linear model (GLM) to fit these counts (response variable) with respect to maternal age and sample type (predictor variables). A model including maternal age as a quadratic predictor variable fit the data significantly better than a reduced model with age as a linear predictor (χ^2 of deviance, $p = 1 \times 10^{-43}$; pseudo-$R^2 = 0.240$).

We note that the improved fit of the quadratic model does not necessarily imply a significant decline in meiotic errors with maternal age in the lower part of the age distribution. To test this hypothesis, we set a maximum threshold on maternal age and fit a quasibinomial GLM to the subset of data from young mothers, including age as a linear predictor. To choose an appropriate age threshold, we performed power calculations using data simulated under binomial models informed by the effects of the full quadratic model. Specifically, for each patient, we used the fitted value from the quadratic model as the probability of "success" (i.e., meiotic error) for *n* random samples from a binomial distribution, where *n* is the number of embryo biopsies from that IVF case. Power was calculated as the proportion of 10,000 simulations in which we rejected the null hypothesis (no maternal age effect) at $\alpha = 0.05$. We repeated this procedure in 0.1 year increments ranging from age 25 to 30 and selected the age that maximized power (27.1 years; power = 0.179) as the preferred age cut-off. The maternal age term achieved nominal significance at this threshold

(β = -0.082, 95% CI [-0.157, 5.88 × 10^{-3}], p = 0.034), though see **fig. S12** for how this result depends on choice of cut-off across the tested range.

13. Data transparency and re-use.

We leveraged several datasets from previously published studies. These are made explicit and cited throughout the text.

14. Data availability and permissions.

All data are available at dbGaP (study #35769) under appropriate Data Use Certification (DUC) agreement in accordance with Danish ethical regulation and General Data Protection Regulation (GDPR).

Sections 6 to 9 in the Methods have been submitted for a D.Phil. at the University of Sussex, UK, by RB. RB owns the copyright and has granted his permission to re-use the text.

15. Funding

ERH was funded by NNF Young Investigator Award (NNF15OC0016662), ERC Consolidator Grant (724718-ReCAP), and support from the DNRF Center Grant (DNRF115). ERH is grateful to the Carlsberg Foundation for imaging equipment for this project (CF15-0232). JG was funded from project grant DFF-FSS (6110-00344B). LJN and collection of oocytes at Warwick were funded from MRC project grant MR/M000664/1. GH received funding from the University of Warwick and University Hospitals Coventry and Warwickshire NHS Trust. APZ and MS received support from the Max Planck Society, the European Research Council (337415), and the Lister Institute for Preventive Medicine. AZ: Rosetrees Trust PhD Fellowship. SGK, MLG, CYA, and ERH are thankful for general support from ReproUnion and Ferring Pharmeceuticals.

16. Author contribution

JRG, APZ, VS and RB performed the majority of the experiments. JRG and VS contributed to fig. 1-3. APZ and MS developed the high-resolution imaging and discovered chromosome threads (fig. 4). RB developed the MDA-NGS technology (fig. 1). DC, DN, LJN, CS, MK, DT, SGK, EE, AMBB, LBC, JL, GH, MLG, KL, MB, KE and CYA conducted clinical coordination. ACHC and IV assisted with genomic analyses. RMC completed the analysis for fig. 1E. ERH conceived the study and analysed the data. JRG and ERH wrote the manuscript. All authors commented and approved the manuscript. Responsibilities for ethics, informed consent and personal data protection are described in Methods section 1.

17. Supplemental materials note

References 30-49 are only used in the supplemental materials.

Full References

1. K. Hawkes, K. R. Smith, Do women stop early? Similarities in fertility decline in humans and chimpanzees. *Ann N Y Acad Sci* **1204**, 43-53 (2010).
2. A. Huseynov *et al.*, Developmental evidence for obstetric adaptation of the human female pelvis. *Proc Natl Acad Sci U S A* **113**, 5227-5232 (2016).
3. A. Kumar, T. Singh, S. Basu, S. Pandey, V. Bhargava, Outcome of teenage pregnancy. *Indian J Pediatr* **74**, 927-931 (2007).
4. P. S. Kim, J. E. Coxworth, K. Hawkes, Increased longevity evolves from grandmothering. *Proc Biol Sci* **279**, 4880-4884 (2012).
5. M. J. Zelazowski *et al.*, Age-Dependent Alterations in Meiotic Recombination Cause Chromosome Segregation Errors in Spermatocytes. *Cell* **171**, 601-614 e613 (2017).
6. A. Capalbo, E. R. Hoffmann, D. Cimadomo, F. Maria Ubaldi, L. Rienzi, Human female meiosis revised: new insights into the mechanisms of chromosome segregation and aneuploidies from advanced genomics and time-lapse imaging. *Hum Reprod Update* **23**, 706-722 (2017).
7. T. Hassold, D. Chiu, Maternal age-specific rates of numerical chromosome abnormalities with special reference to trisomy. *Hum Genet* **70**, 11-17 (1985).
8. L. Escrich *et al.*, Spontaneous in vitro maturation and artificial activation of human germinal vesicle oocytes recovered from stimulated cycles. *J Assist Reprod Genet* **28**, 111-117 (2011).

9. L. Escrich *et al.*, The dynamics of in vitro maturation of germinal vesicle oocytes. *Fertil Steril* **98**, 1147-1151 (2012).
10. R. C. McCoy *et al.*, Evidence of Selection against Complex Mitotic-Origin Aneuploidy during Preimplantation Development. *PLoS Genet* **11**, e1005601 (2015).
11. R. C. McCoy *et al.*, Common variants spanning PLK4 are associated with mitotic-origin aneuploidy in human embryos. *Science* **348**, 235-238 (2015).
12. C. D. Darlington, *Recent advances in cytology*. (P. Blakiston's son & co., inc., Philadelphia,, ed. 2d, 1937), pp. xvi, 671 p.
13. R. R. Angell, Predivision in human oocytes at meiosis I: a mechanism for trisomy formation in man. *Hum Genet* **86**, 383-387 (1991).
14. C. S. Ottolini *et al.*, Tripolar mitosis and partitioning of the genome arrests human preimplantation development in vitro. *Sci Rep* **7**, 9744 (2017).
15. C. S. Ottolini *et al.*, Genome-wide maps of recombination and chromosome segregation in human oocytes and embryos show selection for maternal recombination rates. *Nat Genet* **47**, 727-735 (2015).
16. S. A. Henderson, R. G. Edwards, Chiasma frequency and maternal age in mammals. *Nature* **218**, 22-28 (1968).
17. T. Chiang, F. E. Duncan, K. Schindler, R. M. Schultz, M. A. Lampson, Evidence that weakened centromere cohesion is a leading cause of age-related aneuploidy in oocytes. *Curr Biol* **20**, 1522-1528 (2010).
18. L. M. Lister *et al.*, Age-related meiotic segregation errors in mammalian oocytes are preceded by depletion of cohesin and Sgo2. *Curr Biol* **20**, 1511-1521 (2010).
19. F. E. Duncan *et al.*, Chromosome cohesion decreases in human eggs with advanced maternal age. *Aging Cell* **11**, 1121-1124 (2012).
20. A. P. Zielinska, Z. Holubcova, M. Blayney, K. Elder, M. Schuh, Sister kinetochore splitting and precocious disintegration of bivalents could explain the maternal age effect. *Elife* **4**, (2015).
21. J. Patel, S. L. Tan, G. M. Hartshorne, A. D. McAinsh, Unique geometry of sister kinetochores in human oocytes during meiosis I may explain maternal age-associated increases in chromosomal abnormalities. *Biol Open* **5**, 178-184 (2015).
22. J. Lagirand-Cantaloube *et al.*, Loss of Centromere Cohesion in Aneuploid Human Oocytes Correlates with Decreased Kinetochore Localization of the Sac Proteins Bub1 and Bubr1. *Sci Rep* **7**, 44001 (2017).
23. R. R. Angell, Meiosis I in human oocytes. *Cytogenet Cell Genet* **69**, 266-272 (1995).
24. A. Kouznetsova, L. Lister, M. Nordenskjold, M. Herbert, C. Hoog, Bi-orientation of achiasmatic chromosomes in meiosis I oocytes contributes to aneuploidy in mice. *Nat Genet* **39**, 966-968 (2007).
25. R. Jessberger, Age-related aneuploidy through cohesion exhaustion. *EMBO Rep* **13**, 539-546 (2012).
26. W. D. Gilliland, E. M. Colwell, F. M. Lane, A. A. Snouffer, Behavior of aberrant chromosome configurations in Drosophila melanogaster female meiosis I. *G3 (Bethesda)* **5**, 175-182 (2014).
27. S. Heckmann *et al.*, Alternative meiotic chromatid segregation in the holocentric plant Luzula elegans. *Nat Commun* **5**, 4979 (2014).
28. S. B. Buonomo *et al.*, Disjunction of homologous chromosomes in meiosis I depends on proteolytic cleavage of the meiotic cohesin Rec8 by separin. *Cell* **103**, 387-398 (2000).

29. N. R. Kudo *et al.*, Resolution of chiasmata in oocytes requires separase-mediated proteolysis. *Cell* **126**, 135-146 (2006).
30. C. Y. Andersen, Success and challenges in fertility preservation after ovarian tissue grafting. *Lancet* **385**, 1947-1948 (2015).
31. G. M. Jagiello, M. Ducayen, J. S. Fang, J. Graffeo, Cytogenetic observations in mammalian oocytes. *In Chromosome Today* **Eds. PL. Pearson & K.R. Lewis**, 43-63 (1975).
32. H. W. Michelmann, L. Mettler, Cytogenetic investigations on human oocytes and early human embryonic stages. *Fertil Steril* **43**, 320-322 (1985).
33. R. H. Martin *et al.*, Chromosomal analysis of unfertilized human oocytes. *J Reprod Fertil* **78**, 673-678 (1986).
34. E. B. Prasath *et al.*, First pregnancy and live birth resulting from cryopreserved embryos obtained from in vitro matured oocytes after oophorectomy in an ovarian cancer patient. *Hum Reprod* **29**, 276-278 (2014).
35. P. S. Uzelac, A. A. Delaney, G. L. Christensen, H. C. Bohler, S. T. Nakajima, Live birth following in vitro maturation of oocytes retrieved from extracorporeal ovarian tissue aspiration and embryo cryopreservation for 5 years. *Fertil Steril* **104**, 1258-1260 (2015).
36. I. Segers *et al.*, In vitro maturation (IVM) of oocytes recovered from ovariectomy specimens in the laboratory: a promising "ex vivo" method of oocyte cryopreservation resulting in the first report of an ongoing pregnancy in Europe. *J Assist Reprod Genet* **32**, 1221-1231 (2015).
37. A. Kedem *et al.*, Outcome of immature oocytes collection of 119 cancer patients during ovarian tissue harvesting for fertility preservation. *J Assist Reprod Genet* **35**, 851-856 (2018).
38. J. R. Gruhn, S. G. Kristensen, C. Y. Andersen, E. R. Hoffmann, In Vitro Maturation and Culture of Human Oocytes. *Methods Mol Biol* **1818**, 23-30 (2018).
39. F. M. Ubaldi *et al.*, Reduction of multiple pregnancies in the advanced maternal age population after implementation of an elective single embryo transfer policy coupled with enhanced embryo selection: pre- and post-intervention study. *Hum Reprod* **30**, 2097-2106 (2015).
40. L. Rienzi *et al.*, Embryo development of fresh 'versus' vitrified metaphase II oocytes after ICSI: a prospective randomized sibling-oocyte study. *Hum Reprod* **25**, 66-73 (2010).
41. C. S. Ottolini *et al.*, Generation of meiomaps of genome-wide recombination and chromosome segregation in human oocytes. *Nat Protoc* **11**, 1229-1243 (2016).
42. A. Capalbo *et al.*, Artificial oocyte activation with calcium ionophore does not cause a widespread increase in chromosome segregation errors in the second meiotic division of the oocyte. *Fertil Steril* **105**, 807-814 e802 (2016).
43. R. C. Blanshard, C. Chen, X. S. Xie, E. R. Hoffmann, Single cell genomics to study DNA and chromosome changes in human gametes and embryos. *Methods Cell Biol* **144**, 441-457 (2018).
44. I. Vogel, R. C. Blanshard, E. R. Hoffmann, SureTypeSC - A Random Forest and Gaussian Mixture predictor of high confidence genotypes in single cell data. *Bioinformatics*, (2019).
45. M. Susiarjo, C. Rubio, P. Hunt, Analyzing mammalian female meiosis. *Methods Mol Biol* **558**, 339-354 (2009).
46. A. P. Zielinska, M. Schuh, A microscopy-based approach for studying meiosis in live and fixed human oocytes. *Methods Cell Biol* **145**, 315-333 (2018).

47. R. L. Wasserstein, N. A. Lazar, The ASA's Statement on p-Values: Context, Process, and Purpose. *Am Stat* **70**, 129-131 (2016).
48. R. C. Team (Vienna, Austria, 2018); https://www.R-project.org.
49. J. O'Quigley, R. H. Xu, J. Stare, Explained randomness in proportional hazards models. *Stat Med* **24**, 479-489 (2005).

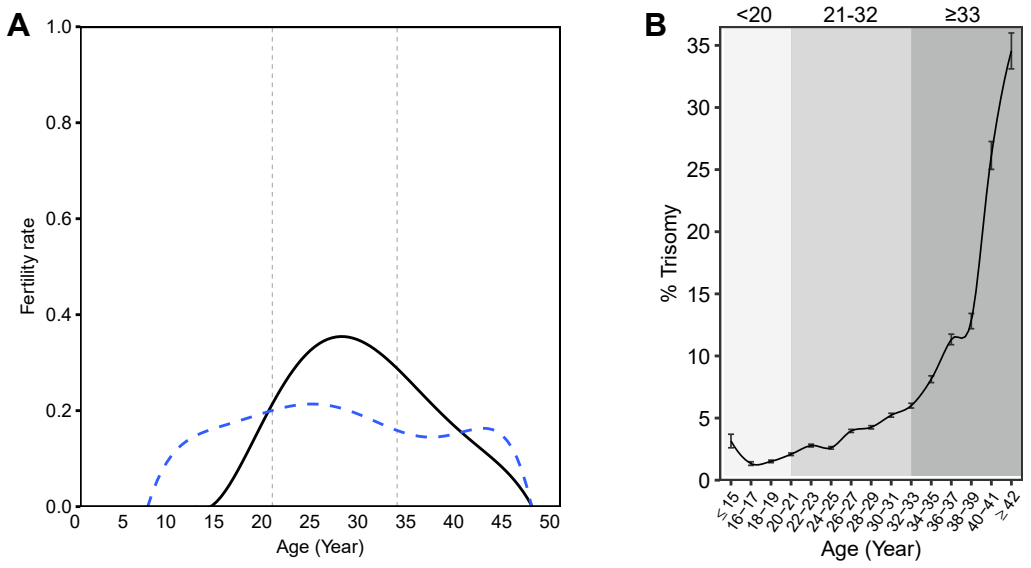

Fig. S1. Incidence of trisomic conceptions in clinically recognised pregnancies. (**A**) Fertility rates of humans (black) and chimpanzees (blue) from ref. 1. Fertility rate calculated as ((Number of live births in specified age group)/(Number in same age group)) x 1000. (**B**) Incidence of trisomy by maternal age from ref. 7. The differentially shaded areas show our three age groups used to study age-related aneuploidy.

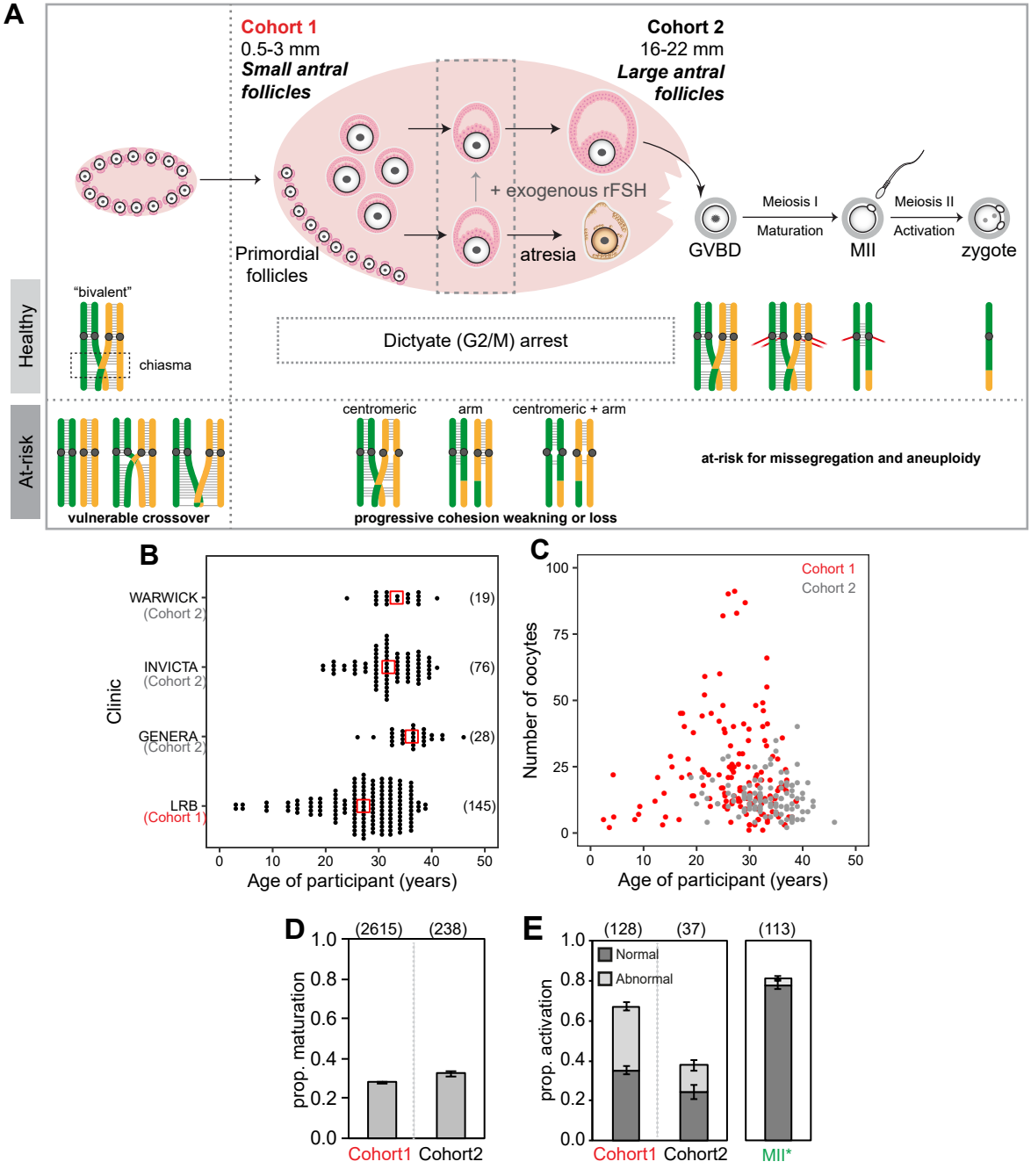

Fig. S2. Meiotic progression in human oocytes. (**A**) Follicular growth in the ovary from fetal, to small antral, and mature follicle stages (above). Female chromosome content during healthy meiosis and at-risk configurations for missegregation (below). Abbreviations: germinal vesicle break down (GVBD), metaphase II arrested (MII), and recombinant follicle stimulating hormone (rFSH). (**B**) Patient ages from each fertility clinic. Participant number in brackets. Red boxes = mean age. (**C**) Oocytes collected per patient in cohort 1 (3,252 GV; red) and cohort 2 (1,201 MII, 186 MI and 272 GV; grey). 84 in vivo matured MIIs were donated and included. (**D**) Maturation rates of 2,615 (cohort 1) and 238 (cohort 2) GVs, respectively. Oocyte number in parentheses. (**E**) Artificial activation rates compared to in vivo mature MII (MII*) oocytes (green). Oocyte number in brackets.

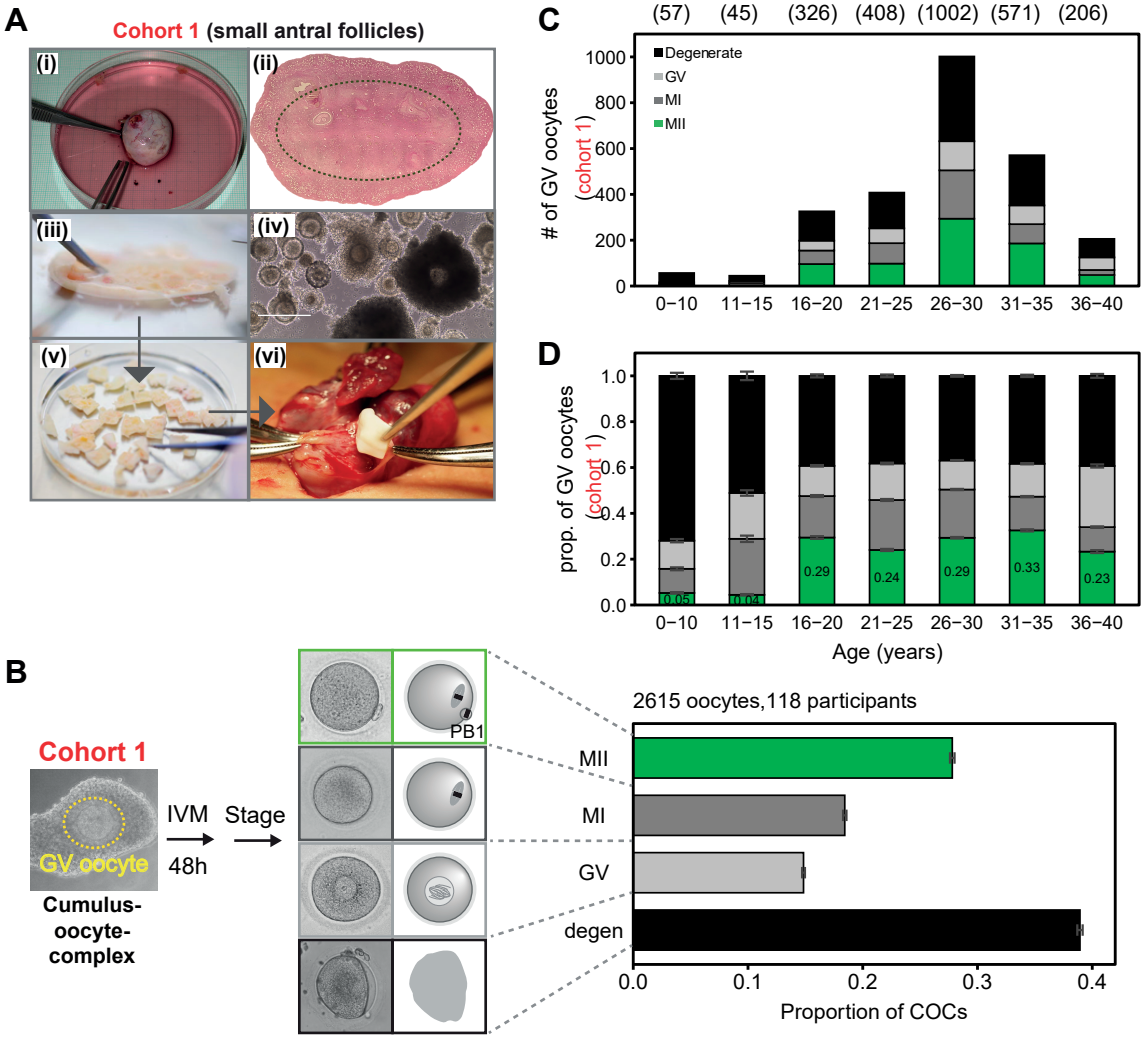

Fig. S3. Maturation of small antral follicles (Cohort 1). (**A**) Collection of oocytes from small antral follicles from ovarian tissue. (i) Human ovaries contain small antral follicles in the medulla (inside the dotted circle; (ii)) from which cumulus-oocyte-complexes are released when the ovarian cortex is prepared for cryopreservation (iii-v). (vi) Autotransplantation of ovarian cortex. Bar (iv): 250 µm. (**B**) Maturation of cumulus-oocyte-complexes from small antral follicles (Cohort 1). After 48 hours, the oocyte was denuded and scored as mature MII by the extrusion of the first polar body (green), MI or failed polar body extrusion by the lack of both a polar body and GV (light grey), GV stage (dark grey), or degenerate, as determined by dark and/or grainy cytoplasm (black). PB1- polar body 1. (**C** and **D**) Maturation rates of oocytes obtained from small antral follicles by age. Error bars: standard error of proportion. Oocyte number in brackets.

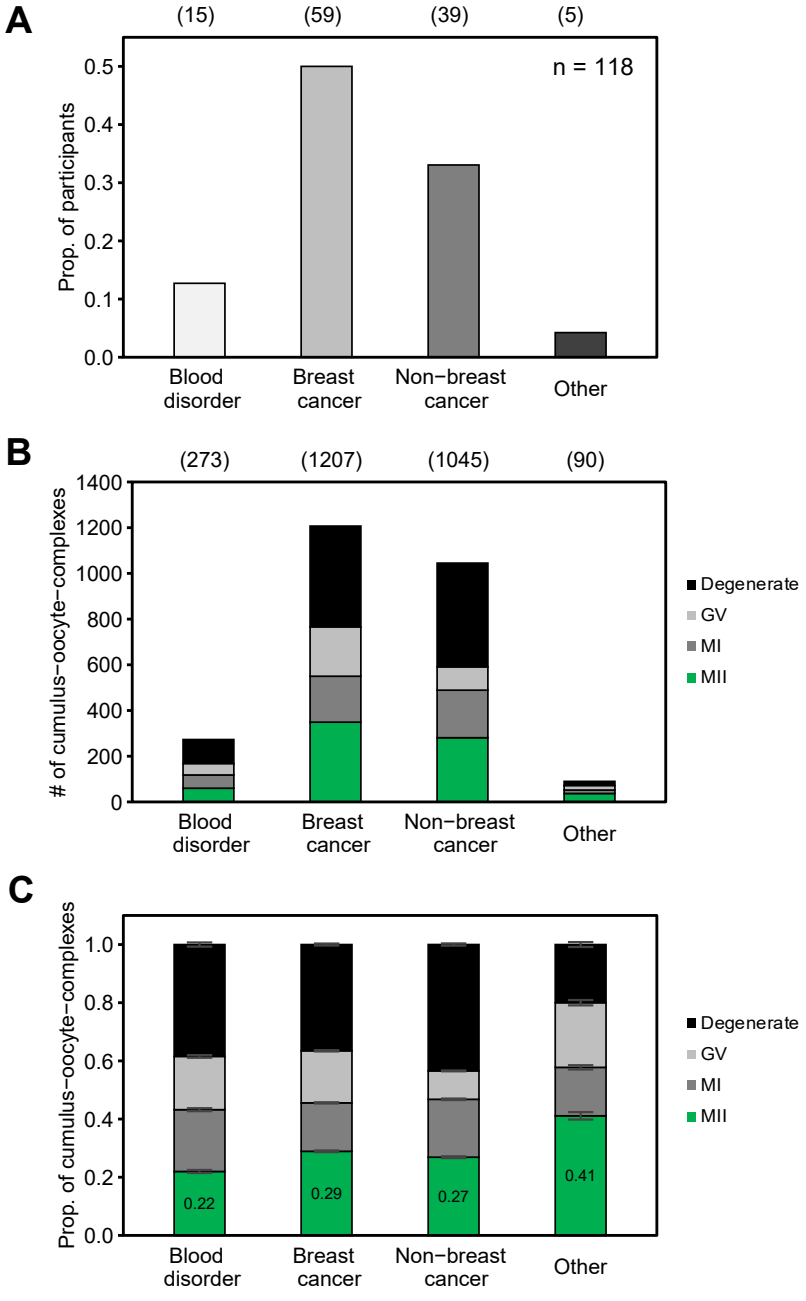

Fig. S4. Maturation rates of GV oocytes obtained from small antral follicles (Cohort 1) by diagnosis. (**A**) Percent of participants by diagnosis. Participant number in brackets. (**B** and **C**) Number and proportion of cumulus-oocyte-complex with mature oocytes (MII), MI, GV or degenerate, grouped by diagnosis. Oocyte number in brackets. Error bars: standard error of a proportion.

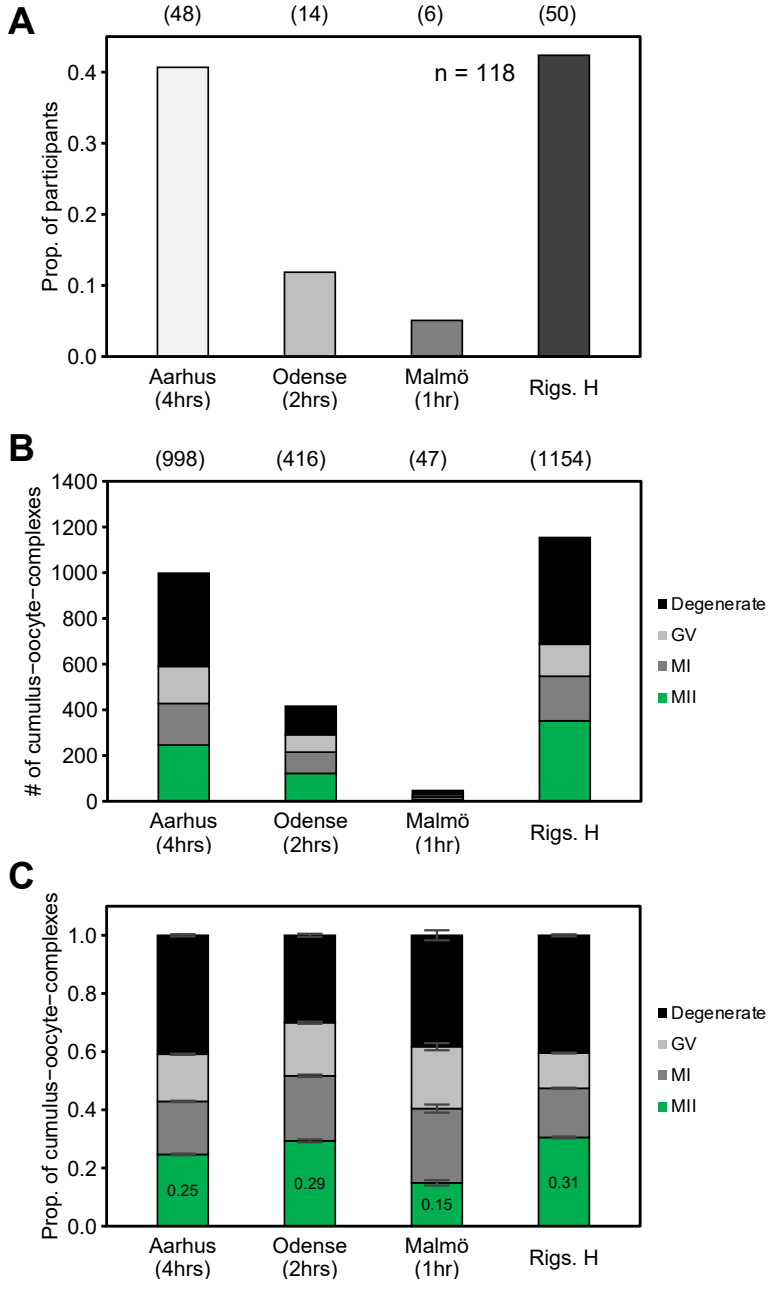

Fig. S5. Maturation rates of GV oocytes from small antral follicles (Cohort 1) by clinic. (**A**) Percent of participants originating from each clinic. Human ovary samples for ovarian cortex cryopreservation were sent from either Aarhus Universitets Sygehus Skejby, Odense Universitets Hospital, Malmö's Akademiske Sygehus, or Rigshospitalet (Rigs.) where the operation took place to the LRB, Rigshospitalet, Copenhagen, Denmark. The time from obtaining the sample to processing is shown on x-axis. Participant number in brackets. (**B** and **C**) Number and proportion of cumulus-oocyte-complexes with mature oocytes (MII), MI, GV or degenerate by collection site. Oocyte number in brackets. Error bars: standard error of a proportion.

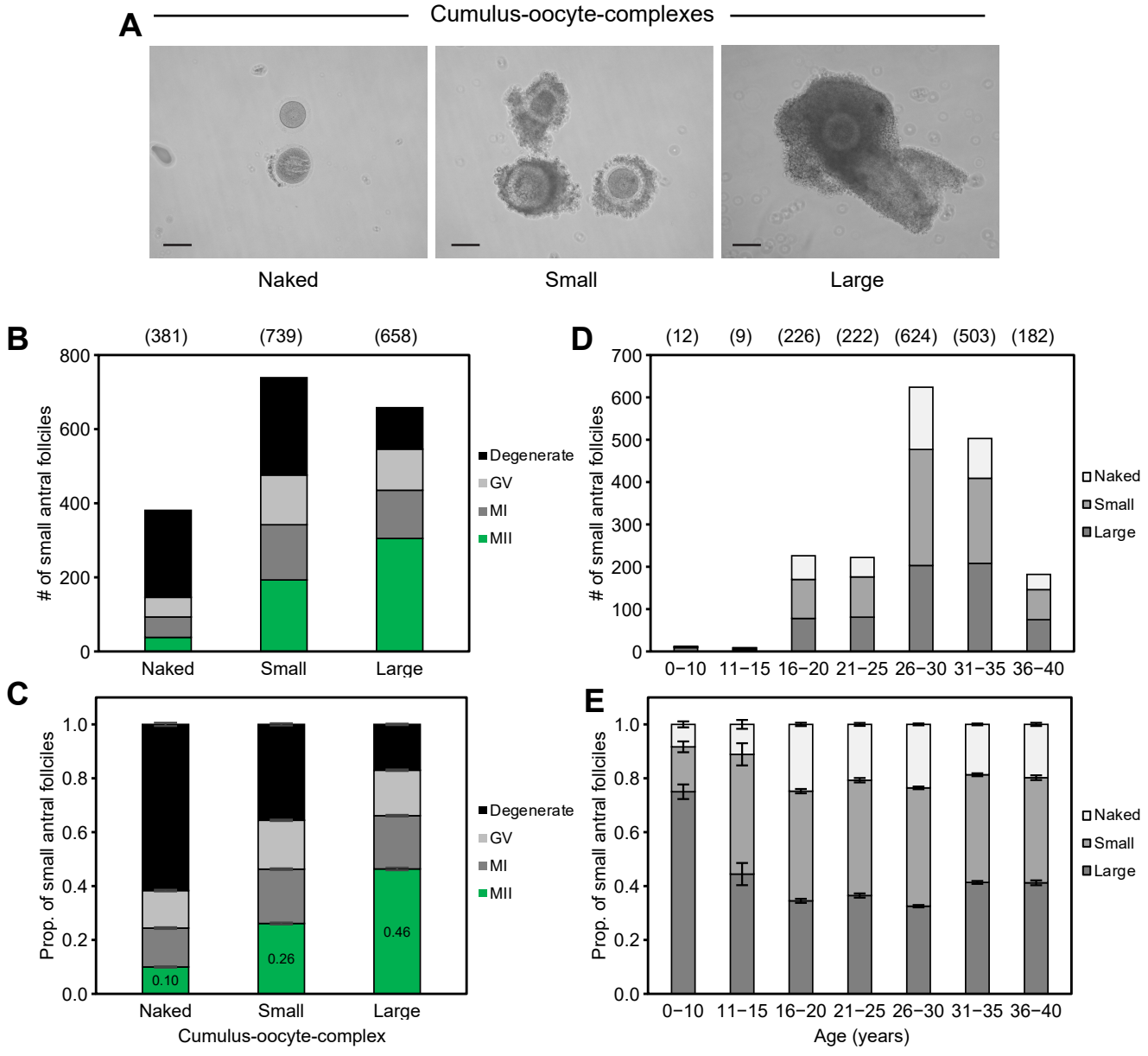

Fig. S6. Maturation rate by morphology and size of cumulus-oocyte-complexes (Cohort 1). (**A**) Images of a naked oocyte, small, and large cumulus-oocyte-complexes. Naked: the oocyte is not surrounded by a complete layer of cumulus cells. Small: oocyte is surrounded completely by approximately 1-4 layers of cumulus cells. Large: oocyte cumulus layer is more than 4 layers of cumulus cells thick. Large cumulus-oocyte-complexes may not completely surround the oocyte due to mechanichal shearing of the thick cumulus cell layer. Scale bar: 100 μm. (**B** and **C**) Maturation outcomes of GV oocytes obtained from small antral follicles by morphology and size (ref. 38). Number of cumulus-oocyte-complexes in brackets. (**D**, **E**) Class of cumulus-oocyte-complex collection by maternal age group. Number of cumulus-oocyte-complexes in brackets. Error bars: standard error of a proportion.

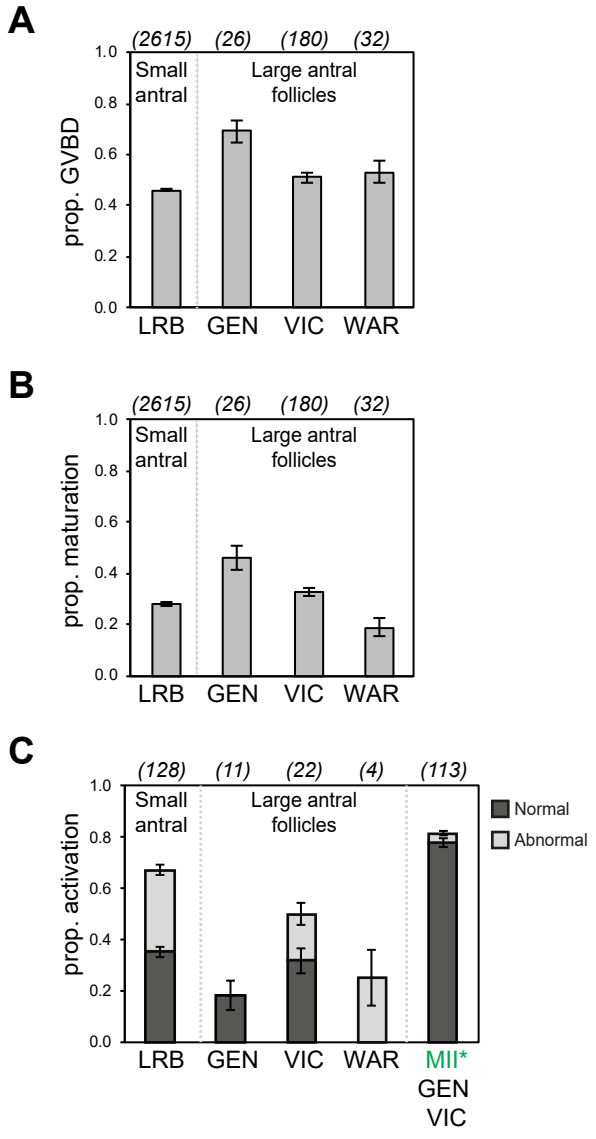

Fig. S7. Completion of meiosis I (maturation) and meiosis II (activation) by clinic. Oocytes from various clinics were at GV stage at collection (identified after stripping of cumulus cells) and were matured to MII. MII* denote oocytes that matured *in vivo* and were clinical grade, but donated for research. The dataset for activation of MII* is a composite from this study as well as ref. 15 and ref. 41. (**A**) Proportion of GV oocytes that underwent GVBD (final maturation stage of either MI or MII). (**B**) Proportion of oocytes that matured (breakdown of GV and extrusion of PB1). (**C**) Proportion of MII oocytes that responded to artificial activation by calcium ionophore A23187. Normal activation in dark grey representing oocytes with extrusion of both PB1 and PB2 and the formation of one (2PB,1PN) or no pronuclei (2PB,0PN). Abnormal activation in light grey representing oocytes that extruded two polar bodies and had two or more pronuclei (2PB,≥2PN), or had a single polar body and more than one pronucleus (1PB,>1PN). Errors bars: standard error of a proportion. Oocyte number in brackets.

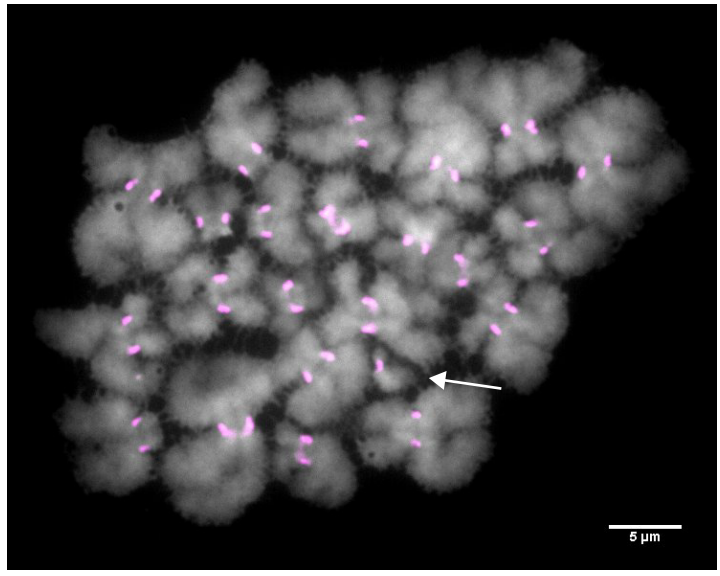

Fig. S8. Chromosome spread from MII oocytes. Chromosomes were labeled with DAPI (gray) and centromeres marked by CREST serum (magenta) to denote chromatin and kinetochores, respectively. The arrow shows example of a single chromatid, lacking its partner. Scale bar: 5 µm. OocyteID: PT951-10 (from cohort 1; small antral follicle).

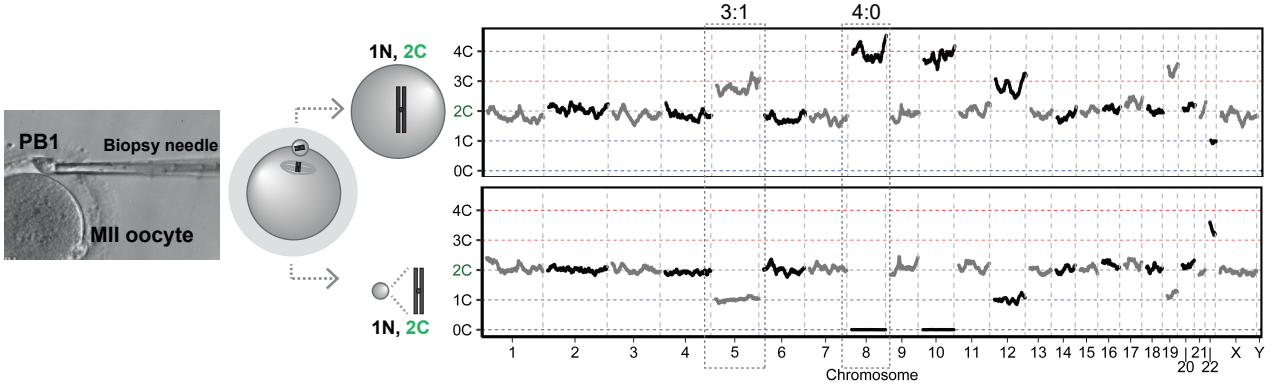

Figure S9. Copy number variation from NGS data. Mature MII oocytes and corresponding biopsied polar body 1 (PB1) underwent whole-genome amplification and NGS. Copy number variation reveals reciprocal gains and losses of single chromatids (3C and 1C) and whole chromosomes (4C and 0C).

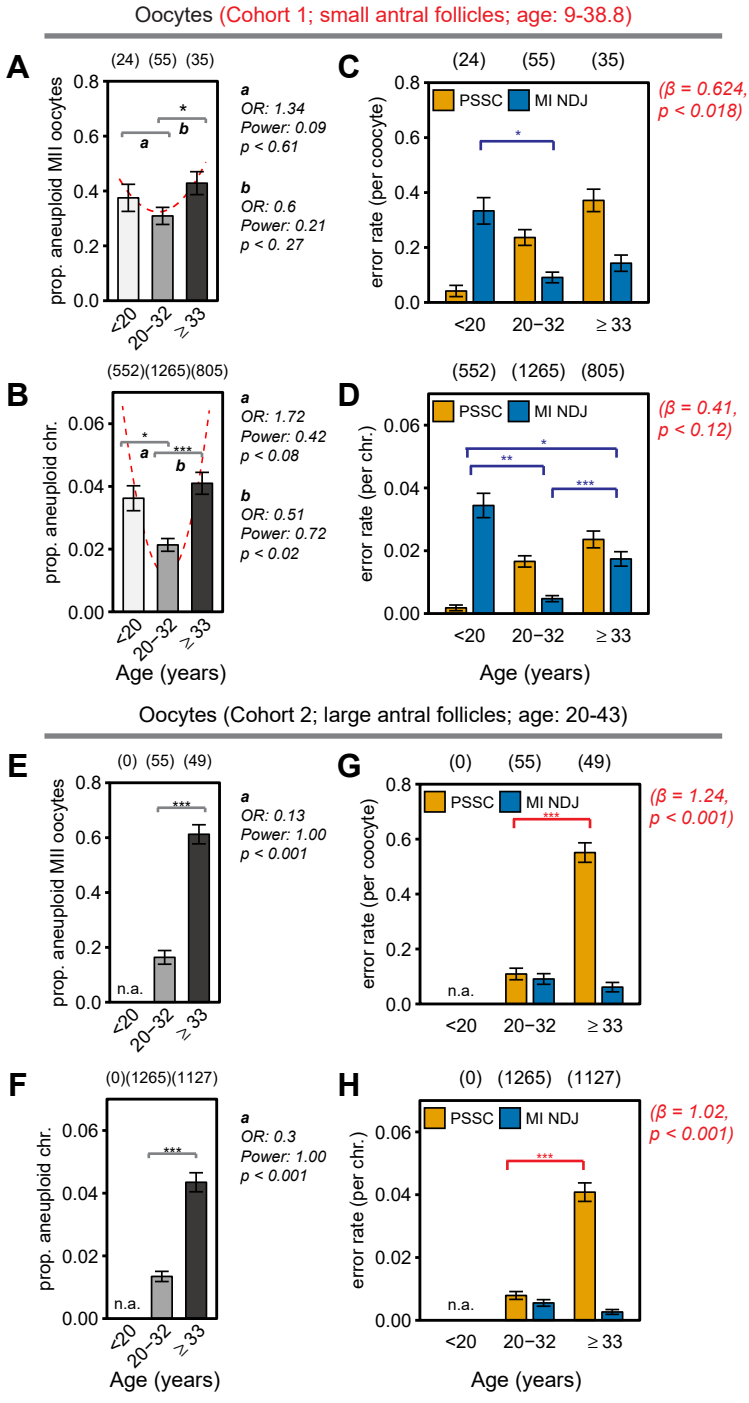

Fig. S10. Meiosis I errors in human oocytes by follicle type. (**A**, **B**) Proportion of aneuploid MII oocytes (A) or chromosomes (B) in oocytes completing meiosis I from small antral follicles. The female ages are binned in to three age groups and compaired pairwise by age group. a and b indicate the statistical comparisons of the age groups. OR: odds ratio (Fisher exact test), power of detection (α=0.05, h was calculated emperically using the arcsin transformation). *p<0.05, **p<0.025, ***p<0.001. The red line shows the fitted curve for the generalized linear models using a quadratic equation, which provided the best fit. The statistics for the glm are shown to the right. (**C**, **D**) Proportion of meiosis I errors per oocyte (C) or chromosome (D). We analysed MI NDJ by age group, whereas PSSC was fitted with a llinear model using age as a continuous variable. The statistcs for the glm is shown to the right in red. (**E**, **F**) Proportion of aneuploid MII oocytes (E) or chromosomes (F) in oocytes from large antral follicles. We did not have females aged under 20. Stars as in (A, B). (**G**, **H**) Proportion of meiosis I errors per oocyte (G) or chromosome (H), by type. Statistcs as in (C, D). Analysis includes both *in vivo* and *in vitro* MII oocytes after gonadotrophin-sitmulation.

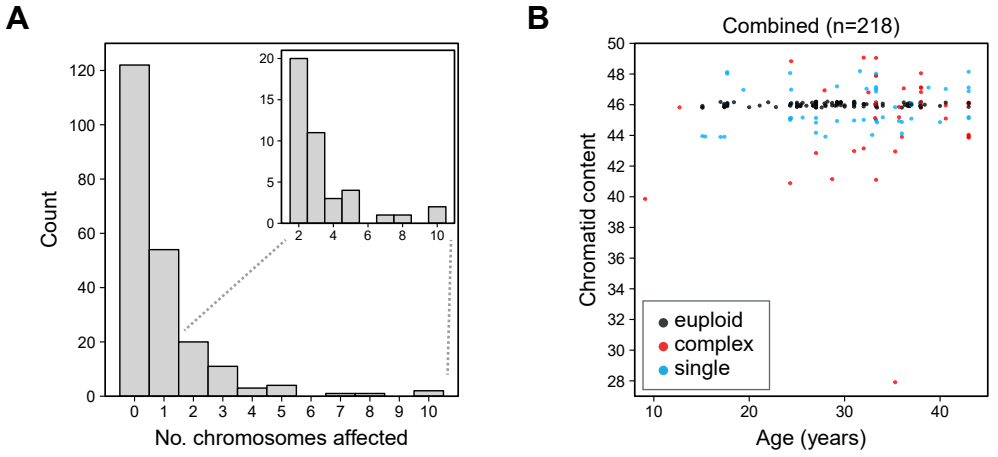

Fig. S11. Complexity of meiosis I segregation errors. (**A**) Oocyte counts of the number of chromosomes affected by MI NDJ, PSSC, or RS. The embedded graph shows zoomed in view of the 2-10 range of affected chromosomes. (**B**) Scatterplot of the number of chromatids or chromosomes affected in each oocyte according to maternal age. Blue: simple aneuploidies. Red: complex aneuploidies where multiple chromosomes are affected.

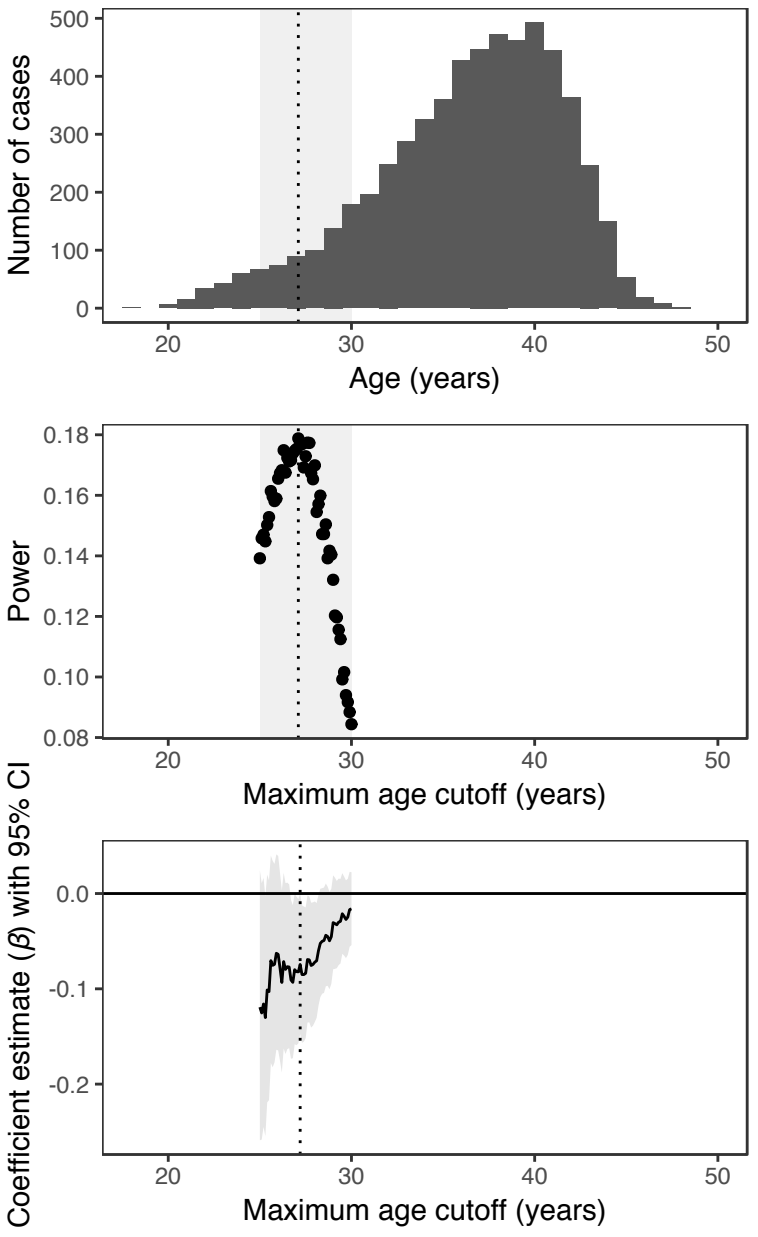

Figure S12. Maternal trisomy analysis from fertilized embryos. The choice of maximum maternal age cutoff was determined using power calculations on simulated data (Methods), varying cutoffs in the maternal age range of 25 to 30 (shaded area) in 0.1 year increments. **Upper panel**: Histogram of maternal age across PGT-A cases. **Middle panel:** Statistical power calculated by fitting linear models to simulated data at varying cutoffs. Maximum power (0.179) was achieved at 27.1 years. **Lower panel**: Coefficient estimates (line) with confidence intervals (shaded area) obtained upon setting the maximum age cutoff at varying values across the tested maternal age range.

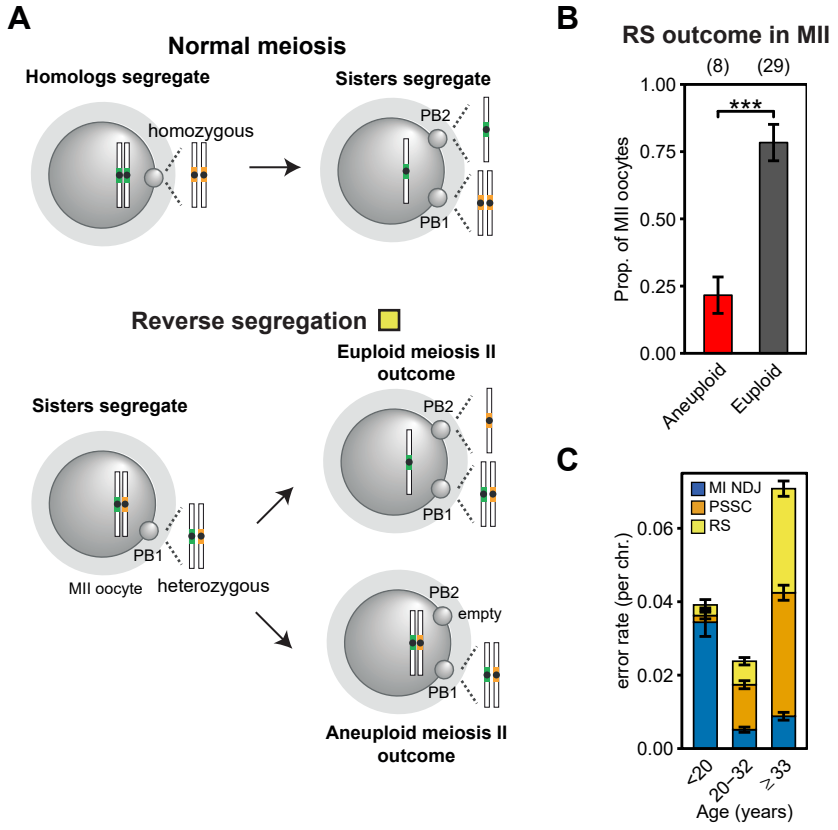

Fig. S13. Reverse segregation. (**A** and **B**) Schematic of reverse segregation and the incidence according to maternal age. Chromosome segregation errors at meiosis II in reverse segregation. Data from 37 events, including 11 events from ref. 14 and 26 from ref. 15. $p < 0.01$ (***). (**C**) Stacked segregation errors by female age including MI NDJ, PSSC, and RS.

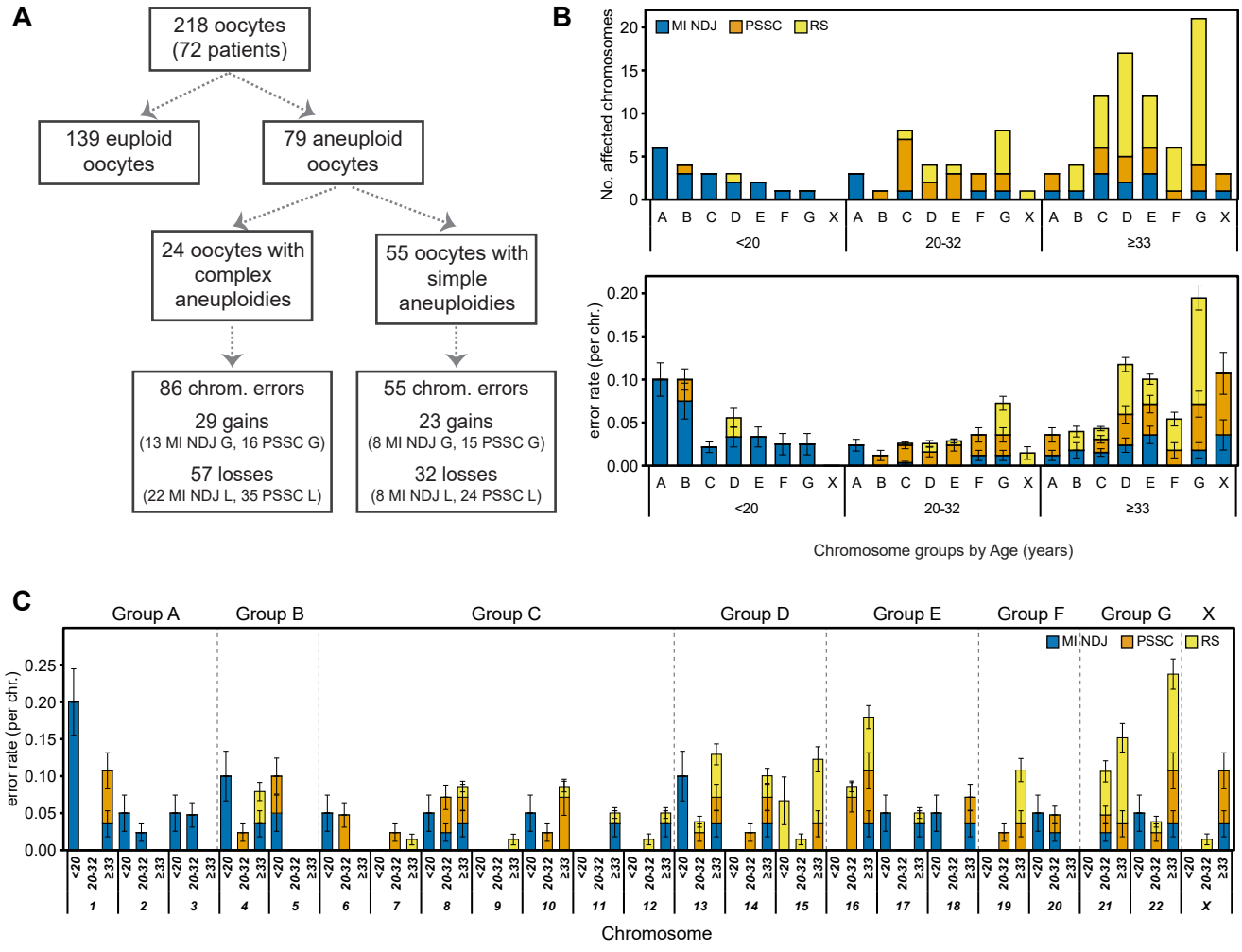

Fig. S14. Aneuploidy patterns. (**A**) Flow diagram describing aneuploid gains (trisomies) and losses (monosomies) in the egg. (**B**) Chromosome errors in meiosis I broken down by maternal age and traditional karyotyping chromosome groups based on size and structure: A (1-3), B (4, 5), C (6-12, X), D (13-15), E (16-18), F (19, 20), and G (21, 22). MI NDJ (blue), PSSC (red), and reverse segregation (yellow). Error bars: standard error of a proportion. (**C**) Further breakdown of chromosome specific error type by chromosome and age. Color scheme and error bars as above.

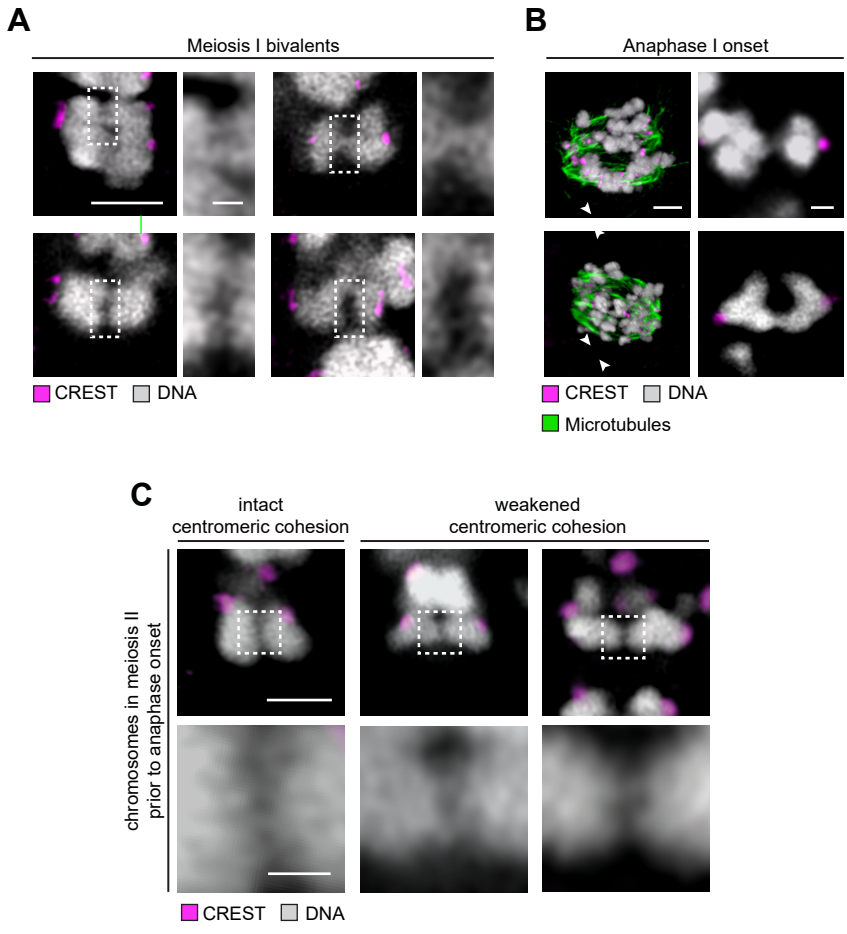

Fig. S15. Chromatin threads between homologs in meiosis I. (**A**) Examples of bivalents with chromatin threads (dotted area). (**B**) Examples of chromatin threads at anaphase I. (**C**) Chromatin threads between chromatids with intact (left panel) and weakened centromeric cohesion. All chromosomes captured prior to anaphase onset. Scale bars: 2 µm (overview) and 0.5 µm (insets).